Fission yeast polycystin Pkd2p promotes transition to cell growth during cytokinesis

Debatrayee Sinha[1], Denisa Ivan[1], Ellie Gibbs[2], Madhurya Chetluru[1], John Goss[2] and Qian Chen[1*]

* Correspondence: qian.chen3@utoledo.edu

[1]: Department of Biological Sciences

University of Toledo

2801 West Bancroft ST

Toledo, OH, 43606

[2]: Department of Biological Sciences

Wellesley College

106 Central Street

Wellesley, MA, 02482

Running title: Pkd2p inhibits SIN, promotes growth

Abbreviations: Atomic force microscopy (AFM), Autosomal dominant polycystic kidney disease (ADPKD), Morphogenesis Orb6 related (MOR), Septation initiation network (SIN), Spindle pole bodies (SPBs)

Summary statement

Mutations in polycystins lead to a human genetic disorder, ADPKD. Our study shows that the fission yeast polycystin homologue Pkd2p plays a distinct role in cytokinesis through opposing the Hippo pathway and promoting cell size growth. (200 characters)

Abstract

Polycystins are evolutionarily conserved cation channels. Mutations of human polycystins lead to a common genetic disorder, Autosomal Dominant Polycystic Kidney Disorder (ADPKD). Interestingly, the fission yeast homologue Pkd2p is required for cytokinesis, the last stage of cell division, but the mechanism remains unclear. Here, motivated by our discovery of the epistatic genetic interactions between *pkd2* and the Hippo pathway Septation Initiation Network (SIN), we investigated their interplay during cytokinesis. We found that *pkd2* modulated the localization as well as the activities of SIN proteins. Most notably, *pkd2* promotes a transition to cell size growth during cytokinesis, which is opposed by SIN. The role of Pkd2p in cell growth is not limited to cytokinesis. A newly isolated *pkd2* temperature-sensitive mutant blocked the cell size expansion during interphase. Such growth defect was accompanied by frequent cell shrinking, reduced cell volume, and decreased cell stiffness. We conclude that Pkd2p promotes transition to the post-mitosis cell size growth in coordination with the Hippo pathway. (160 words)

Introduction

Cytokinesis is the last stage of cell division when two daughter cells separate. During this process, an actomyosin contractile ring assembles at the medial division plane. The ring provides the mechanical force required to drive the membrane ingression, leading to cell separation. Fission yeast, *Schizosaccharomyces pombe*, is an excellent model organism to study this essential cellular process. A large number of cytokinetic mutants have been identified in this model organism. Genetic and cell biology studies have revealed many of the key components, most of which are conserved in metazoans (for a review, see (Pollard and Wu, 2010)).

The fission yeast Hippo pathway SIN (septation initiation network) plays a central role in the signaling cascade that regulates cytokinesis. The metazoan Hippo tumor suppressor pathway consists of a kinase cascade (for a review see (Yu et al., 2015)) and the downstream effector of the transcription factors YAP/TAZ (Huang et al., 2005). It plays an essential role in modulating cell growth and organ size (Camargo et al., 2007; Dong et al., 2007). SIN consists of more than a dozen essential genes (for reviews, see (Johnson et al., 2012; Simanis, 2015)). At the top of this hierarchy is a GTPase Spg1p, localized at the spindle pole bodies (SPBs) throughout mitosis (Schmidt et al., 1997). Its activation propagates the SIN signal through a cascade of three kinases. At the bottom is a nuclear Dbf2-related (NDR) family kinase Sid2p, the homologue of human LATS kinase, which targets many essential cytokinetic proteins (Bohnert et al., 2013; Hergovich, 2016; Sparks et al., 1999; Willet et al., 2019). The activity of SIN in cytokinesis is modulated by MOR (Morphogenesis Orb6 Related), which promotes cell growth through another essential NDR kinase Orb6p (Ray et al., 2010; Verde et al., 1998).

Our recent study has identified another component of the cytokinesis signaling network Pkd2p, the fission yeast homologue of polycystin channels (Morris et al., 2019). Polycystins are conserved in most eukaryotes, even though they were discovered through the genetic studies of one of the most common human genetic disorders, ADPKD (Hughes et al., 1995; Mochizuki et al., 1996). Mutations of human polycystins are the main causes of almost all ADPKD cases, but the mechanism remains unclear. This has resulted in intensive studies of this family of transmembrane proteins over the last two decades (for recent reviews see (Hardy and Tsiokas, 2020; Ta et al., 2020)). Electrophysiological and structural studies have revealed that most polycystins are calcium-permissive cation channels that are closely associated with the primary

cilium in ciliated cells (Gonzalez-Perrett et al., 2001; Hanaoka et al., 2000; Liu et al., 2018; Su et al., 2018). However, their functions have turned out to be surprisingly diverse. While the fruit fly and worm polycystins are essential for male fertility (Barr and Sternberg, 1999; Watnick et al., 2003), the polycystin of the green algae *Chlamydomonas reinhardtii* plays a non-essential structural role in the cilia (Huang et al., 2007; Liu et al., 2020; Wood et al., 2012). In comparison, the polycystin homologue of social amoebae *Dictyostelium discoideum* contributes to cell locomotion (Lima et al., 2014). Nevertheless, the molecular mechanism of these cellular functions has remained elusive, including that of human polycystins.

Similar to the aforementioned unicellular organisms, fission yeast possesses just one homologue of the polycystin channel (Palmer et al., 2005). Pkd2p localizes to the plasma membrane in a cell-cycle-dependent manner. It concentrates at the cell tips during interphase and the cleavage furrow during cytokinesis (Morris et al., 2019). Knock-down of this essential gene leads to mis-regulation of the contractile ring constriction and failed cell separation (Morris et al., 2019). However, the molecular mechanism underlying the function of Pkd2p in cytokinesis remains unclear.

Here we investigated the functional relationship between *pkd2* and SIN during cytokinesis. We first discovered their epistatic genetic interaction through a targeted genetic screen. We demonstrated that *pkd2* modulated both the localization and activities of SIN. *pkd2* opposed the activity of SIN most strongly for the transition to cell size growth during cytokinesis. Such activity of Pkd2p is further examined by characterizing a novel temperature-sensitive *pkd2* mutant. It showed that Pkd2p is equally essential for promoting cell size growth during interphase by maintaining cell stiffness.

Results:

Genetic interactions between SIN and *pkd2* mutants

To understand the role of *pkd2* in fission yeast cytokinesis, we carried out a genetic screen to identify the interactions between a *pkd2* mutant and a collection of more than thirty cytokinetic mutants. *pkd2-81KD* is a hypomorphic mutant in which the expression of *pkd2* is suppressed by replacing the endogenous promoter with a weak promoter P81nmt1 (Morris et al., 2019). Among the mutants that we examined (Table S1 and Morris et al., 2019), two SIN mutants *sid2-250* and *mob1-R4*, exhibited the strongest genetic interaction with *pkd2-81KD* (Morris et al.,

2019). The *pkd2* mutation rescued the viability of these two SIN mutants at semi-permissive temperatures. This discovery prompted us to systematically determine the epistatic relationship between *pkd2* and SIN. We examined the genetic interactions between *pkd2-81KD* and seven other SIN mutants (Fig. 1A–B, S1A, and Table S1). Like the *mob1* and *sid2* mutants, three others including those of *spg1*, *sid4*, and *cdc14* interacted positively with *pkd2-81KD* (Table S1, Fig. 1B), while three others showed no genetic interaction (Table S1, Fig. S1A). Unlike the SIN mutants examined above, *cdc16-116* results in hyperactive SIN signaling (Fankhauser et al., 1993; Furge et al., 1998). It interacted negatively with *pkd2-81KD* (Fig. 1C). The *pkd2* and *cdc16* double mutant was less viable even at the semi-permissive temperature, compared to the *cdc16* mutant. Combined, our genetic analyses suggested an antagonistic relationship between *pkd2* and the SIN pathway in their regulation of cytokinesis.

Since both Pkd2p and some of the SIN proteins localize to the medial division plane (Morris et al., 2019; Salimova et al., 2000; Sparks et al., 1999), we first tested whether Pkd2p directly regulated the intracellular localization of these SIN proteins during cytokinesis. We used quantitative fluorescence microscopy to measure the number of Sid2p and Mob1p molecules throughout cytokinesis. Fission yeast cytokinesis consists of three consecutive stages contractile ring assembly and maturation, ring constriction, and daughter cell separation (Fig. 2A) (Wu et al., 2003). Each lasts ~30 minutes (30′) in the wild-type cells at room temperature, relative to the start of prometaphase marked by the separation of spindle pole bodies (SPBs) (Chen and Pollard, 2011; Morris et al., 2019; Wu et al., 2006). As shown before (Goss et al., 2014), both Sid2p-GFP and Mob1p-GFP localized to the medial division plane throughout the ring constriction (Fig. 2B and S1B). They appeared at the division plane ~20′ after the separation of SPBs (0′). Their numbers increased gradually before peaking at 40′. Both SIN proteins eventually dissipated from the medial plane at the end of the ring constriction (60′). In comparison, such kinetics, as well as the numbers of these two molecules at the division plane, did not change notably in the *pkd2-81KD* cells (Fig. 2B and S1B). The only significant difference was that the peak number of Mob1p-GFP molecules increased by 15% in the mutant cells (Fig 2B–C). In addition to the division plane, both Sid2p and Mobp1 also localized to the SPBs throughout cytokinesis. Compared to the wild-type, the numbers of these two SIN proteins at SPBs almost doubled in the mutant, during the cell separation (60′–90′) (Fig 2B, 2D, S1B). Even after cell separation, Mob1p-GFP continued to dwell on the SPBs of the mutant cell longer (+20′), compared to the

wild-type (Fig S1C). We concluded that Pkd2p modulated the cytokinetic localization of both Sid2p and Mob1p.

Next, we determined whether Pkd2p can directly inhibit the SIN activities. SIN plays several essential cytokinetic roles. Here we were focused on its activity in regulating the localization of Cdc7p, septation, and daughter cell integrity.

First, we examined how Pkd2p regulates the asymmetric localization of the SIN kinase Cdc7p to the SPBs (Sohrmann et al., 1998) (Fig. 3A). We measured the dwell time of Cdc7p-GFP on the two SPBs with time-lapse microscopy. In wild-type cells, Cdc7p-GFP remained at one SPB (new) for ~50 minutes, from the start of prometaphase through the end of telophase (Fig. 3A, S1D). In comparison, its localization at the other SPB (old) lasted only ~15 minutes (Fig. 3A, S1D), consistent with the previous measurements (Dey and Pollard, 2018). We quantified this SIN activity as the ratio of the dwell times of Cdc7p on the two SPBs (old:new). It averaged ~0.29 for the wild-type cells (Fig. 3B). When SIN is hyperactive, this value would increase to ~1.0 (Dey and Pollard, 2018). The value increased by 33% in the *pkd2-81KD* mutant cells (Fig. 3B). It was mostly due to the increased dwell time of Cdc7p-GFP at the old SPB (Fig. S1D). We concluded that *pkd2* modestly modulates the SIN activity as measured by the localization of Cdc7p.

Secondly, we examined how Pkd2p regulates the SIN activity of promoting septation. During fission yeast cytokinesis, the formation of the septum requires SIN. As shown in previous studies (Balasubramanian et al., 1998), most SIN mutants failed to form the septum at the restrictive temperature (Fig. 3C). This defect was rescued by the *pkd2-81KD* mutation in 6 out of 8 SIN mutants (Fig. 3C). The exceptions were the *cdc7* and *sid1* mutants (Fig. 3C). The most significant effect was found in the *cdc11* mutant, in which the septation index increased from 1% to 17% by the *pkd2* mutation, but many of these septa were thin or partially assembled. We concluded that *pkd2* also modestly modulates the SIN activity measured in septation.

Lastly, we tested how Pkd2p regulates the SIN activity of keeping daughter cells intact. Although less understood, SIN also ensures the integrity of separating cells and prevent their lysis. Consistent with the previous studies (Garcia-Cortes and McCollum, 2009; Gupta et al., 2014; Jin et al., 2006), we found that all SIN mutants lysed at the restrictive temperature, but in varying degrees ranging from 12% (*sid1-125*) to 52% (*cdc14-118*) (Fig. 3D). The *pkd2-81KD*

mutation reduced the fraction of lysed cells to less than 5% for all SIN mutants, except for the *sid1* mutant (Fig. 3D). The lysis of the *cdc14* mutant decreased most drastically, by more than 10-folds from 52% to just 3% (Fig. 3D). We concluded that *pkd2* strongly modulates the SIN activity of maintaining cell integrity.

Collectively, among the three SIN activities that we measured, *pkd2-81KD* most strongly rescued SIN mutants by preventing the daughter cells from lysis. This suggested a model in which *pkd2* promotes the cell size expansion which is modulated by SIN to prevent lysis. Hence, we proceeded to test this model in the rest of this study.

Isolation of a novel *pkd2* temperature-sensitive mutant

The above results prompted us to isolate new *pkd2* mutants to examine its role in cell size growth, as the available mutant *pkd2-81KD* exhibited only a minor growth defect (Morris et al., 2019). Through a genetic screen, we identified a novel temperature-sensitive mutant, *pkd2-B42*. The mutant allele contained eight missense mutations, within the sequence of the transmembrane helices 3–9 (Fig. 4A and Table S2). This mutant was inviable at the restrictive temperature of 36°C or above (Fig. 4B). Its temperature sensitivity was not rescued by the supplementation of sorbitol in the media (Fig. 4C). The mutant was hypersensitive to calcium, similar to *pkd2-81KD* (Fig. 4D). Most importantly, this mutant grew much slower than either the wild-type or *pkd2-81KD* at the restrictive temperature (Fig. 4E).

The *pkd2-B42* mutant cells exhibited serious morphological and polarity defects. They were significantly shorter and wider than the wild-type cells at the restrictive temperature (Fig. S2A–B). Many were deflated at 36°C, accompanied by reduced size and denser cytoplasm (Fig. 4F). The fraction of such deflated cells increased when incubated at 36°C, reaching ~50% after 8 hours (Fig. 4G). In the mutant cells, a large number of actin patches appeared outside of the growth zones (cell tips or the division plane), unlike wild-type cells (Fig. S2C). Nevertheless, the polarity of this *pkd2* mutant as measured by CRIB-mCherry, a fluorescence indicator for active Cdc42p (Tatebe et al., 2008), remained largely unchanged from the wild-type (Fig. S2D). Interestingly, the polarity indicator diffused throughout the cytoplasm of almost half of the mutant cells, which was never observed in the wild-type cells (Fig. S2D–E). We concluded that this novel temperature-sensitive *pkd2-B42* mutant allele impairs cell morphogenesis.

Next, we determined whether *pkd2-B42* interacted with the SIN mutants genetically as *pkd2-81KD* did. *pkd2-B42* exhibited positive interactions with three SIN mutants we tested, including those of *sid2, mob1* or *spg1* (Fig. 5A and Fig. S3A). This *pkd2* mutant allele significantly increased the septation indices of both *sid2* and *mob1* mutant cells at the restrictive temperature to 22% and 47% respectively (Fig. 5B). It also drastically reduced the percentage of tetra-nucleated cells, a signature SIN phenotype, from 90% to 7% in *sid2-250* (Fig. S3B). In addition, *pkd2-B42* reduced the percentiles of lysed SIN mutant cells to less than 2%, from 17% (*sid2-250*) and 66% (*mob1-R4*) at 36°C (Fig. 5C). Thus, this novel *pkd2* mutant allele also confirmed the antagonism between *pkd2* and SIN.

Such a relationship between SIN and *pkd2* bears a strong resemblance to that between SIN and MOR, prompting us to investigate the relationship between *pkd2* and MOR. The MOR pathway antagonizes SIN during cytokinesis and promotes cell growth (Gupta et al., 2013; Ray et al., 2010; Verde et al., 1998). Similar to the *pkd2* mutants, the MOR mutant *orb6-25* prevented the SIN mutant *mob1-R4* from lysis (Fig. 6A). They exhibited negative genetic interactions with *pkd2-B42* (Fig. 6B). The MOR mutant cells are spherical or orb-shaped at the restrictive temperature due to defective polarized cell growth (Verde et al., 1998). In comparison, both *orb6 pkd2* and *mor2 pkd2* mutant cells reassembled more closely to the *pkd2-B42* mutant cells (Fig. 6C–D). However, compared to the *pkd2* mutant cells, a larger fraction of *orb6 pkd2* and *mor2 pkd2* mutant cells became deflated at the restrictive temperature (Fig. 6C and 6E). We concluded that *pkd2* and MOR act synergistically in promoting cell size growth.

The role of *pkd2* in interphase cell growth

The critical role of Pkd2p in promoting the transition to cell growth during cytokinesis led to our next question, whether it is also required for interphase growth. The rod-shaped fission yeast cells grow exclusively by expanding their tips until reaching ~14µm to enter mitosis. First, we measured the rate of tip growth using time-lapse microscopy. At the permissive temperature, the *pkd2-B42* mutant cells expanded at a rate of ~2 µm/hour, similar to the wild-type cells (Fig. 7A). However, at the restrictive temperature of 37°C, the expansion of the mutant cells slowed down drastically to a rate of less than 1µm/hour, while that of the wild-type cells increased to close to 4µm/hour (Fig. 7A–B, Movie S1 and S2). Not only did the mutant cells expanded their tip much slower, but they also grew with frequent pauses (66%, n = 229) (Fig. 7B–C). The pauses were

concurrent with a temporary deflation that usually lasted ~20 minutes (16 ± 7 mins, average ± SD, n = 152) (Fig. 7C, Movie S3). The slow tip expansion of *pkd2-B42* cells led to the prediction that they would take much longer to reach the minimum length required for mitotic entry, compared to the wild-type cells. As expected, less than 1% of the mutant cells were in mitosis at the restrictive temperature, far less than the wild-type (8%) (Fig. 7D–E). We concluded that Pkd2p promotes tip expansion during interphase growth.

Next, we determined whether Pkd2p is required for the three-dimensional volume expansion of fission yeast cells. Although it remains technically challenging to directly measure the volume of a single fission yeast cell, we adopted a novel fluorescence microscopy-based approach for indirect measurement (Knapp et al., 2019). The cellular concentration of a constitutively expressed fluorescence protein is used as the indicator of the cell volume. Assuming that biosynthesis of such fluorescence proteins is coupled with cell volume expansion, the fluorescence of yeast cells shall remain constant throughout the cell cycle. However, a defect in volume expansion results in an elevated concentration of the fluorescence protein, increasing intracellular fluorescence (Knapp et al., 2019). We compared the wild-type and *pkd2* mutant cells, both constitutively expressing GFP (super-fold GFP), with quantitative fluorescence microscopy. As expected, the average fluorescence of the wild-type cells clustered around the average value, even among an asynchronous population of cells (Fig. S4A–B). In comparison, the average fluorescence of *pkd2-B42* cells was ~50% higher, exhibiting a bimodal distribution (Fig. S4B). Similar to the *pkd2* mutant, the MOR mutant *orb6-25* expressing GFP doubled its intracellular fluorescence at the restrictive temperature, compared to wild-type (Fig. S4B). Those temporarily shrunken *pkd2* mutant cells exhibited relatively lower fluorescence compared to the others (Fig. S4B'). Thus, we confirmed that Pkd2p is required for the volume expansion of fission yeast cells throughout the cell cycle.

To understand how Pkd2p promotes cell size expansion, we tested whether it regulates the turgor pressure that is essential for such growth. As an indirect measurement of the turgor pressure, we quantified cell stiffness with atomic force microscopy (AFM) (Gibbs et al., 2021). AFM is a scanning probe experimental tool that can provide topographical images at nanoscale resolution and characterize the nanomechanical biophysical properties of cellular surfaces (for a review see (Goss and Volle, 2020)). We probed the cells with AFM to acquire force-distance

curves of surface indentation and cellular spring constants (Fig. 8A–E). The cellular spring constant of wild-type cells was 42 ± 10 mN/m (average ± S.D.), consistent with previously reported values (Gibbs et al, 2021). In comparison, the spring constant of *pkd2-B42* mutant cells was 40% lower at the permissive temperature (26 ± 12 mN/m) (Fig. 8F). It decreased further to 16 ± 11 mN/m at the restrictive temperature, 60% lower than the wild-type cells (40 ± 12 mN/m) (Fig. 8F). Comparably, the spring constant of the other *pkd2* mutant *pkd2-81KD* was between those of *pkd2-B42* and the wild type. Thus, we concluded that *pkd2* is essential for maintaining cell stiffness during cell size growth.

Discussion:

Cytokinesis is defined by the physical separation of daughter cells, but it is also when a transition to resume cell growth starts. Such transition has often been overlooked due to the challenges of measuring cell growth accurately during this period. Recent technical advances however have demonstrated that animal cell cytokinesis is accompanied by the growth of both biomass (Miettinen et al., 2019) and cell size/volume (Li et al., 2017). Similar growth transition occurs in fission yeast cytokinesis as well. It includes, but is not limited to, the biomass increases in the form of septum biosynthesis and the size expansion in the form of a new tip for each daughter cell. The molecular mechanism of such growth transition nevertheless remains poorly understood. Here, our study demonstrates that the fission yeast Hippo pathway SIN and the putative mechanosensitive channel Pkd2p jointly regulate such transition. Specifically, SIN delays the cell size expansion while Pkd2p promotes it. The growth-promoting activity of this putative transient receptor potential (TRP) channel extends into the interphase growth as well. We propose that Pkd2p directly regulates the homeostasis of intracellular osmolarity to promote size expansion throughout the cell cycle.

Functional antagonism between SIN and *pkd2* during cytokinesis

The most striking demonstration of the relationship between *pkd2* and SIN is that mutations of *pkd2* almost completely prevented SIN mutant cells from lysis. Based upon our proposed role for Pkd2p, this would suggest that SIN plays a previously overlooked role in inhibiting cell size expansion. This SIN activity would be comparable to that of the metazoan Hippo tumor suppressor pathway which modulates the tissue size growth (Dong et al., 2007; Pan, 2007). It is still entirely unclear how SIN executes such a function. At the minimum, it can do so directly by

inhibiting the growth-promoting MOR pathway (Gupta et al., 2013; Ray et al., 2010). However, the MOR mutations did not completely prevent the lysis of SIN mutants as the *pkd2* mutations did. Therefore, SIN may have additional targets in its inhibition of the cell size growth besides MOR. The recent finding that the mammalian polycystin PC-1 modulates the activity of the Hippo pathway in the kidney cells (Cai et al., 2018) suggests that the antagonism between polycystin and the Hippo pathway may be evolutionally conserved.

Two other SIN phenotypes are also suppressed by the *pkd2* mutations albeit only partially. The *pkd2* mutations allowed the SIN mutant cells to synthesize many incomplete or thin septum. This may have been facilitated by the reduced intracellular osmolarity. Secondly, the fraction of multi-nucleate SIN mutants including those with four nuclei was significantly reduced by the *pkd2-B42* allele. We consider this an indirect result of the slow interphase growth due to the *pkd2* mutation. The *pkd2* SIN double mutant may be growing too slowly to reach the length required for the mitotic entry within the 4-hour window at the restrictive temperature.

Overall, inactivation of Pkd2p only partially rescued the viability of SIN mutants. This is consistent with that SIN is required for many other functions during cytokinesis besides inhibiting the growth transition. We also noticed that mutations of *pkd2* did not rescue all the SIN mutants to the same extent. The most notable exception is the *sid1* mutant. It exhibited no genetic interaction with the *pkd2* mutant. Neither septation nor lysis defect of the *sid1-125* mutant cells was rescued by *pkd2-81KD* mutation. This stood in stark contrast to the mutants of either *cdc7* or *sid2*, two other essential kinases of SIN. This suggests that Sid1p may have a different role from the other two kinases in the growth transition during cytokinesis.

Depletion of *pkd2* increased the cytokinetic localization of the SIN proteins modestly but significantly, especially at the SPBs. This is surprising because Pkd2p itself does not localize to the SPBs. On contrary, it localizes at the cleavage furrow throughout cytokinesis (Morris et al., 2019). Therefore, we consider it more likely that Pkd2p indirectly regulates the localization of SIN proteins by regulating the intracellular calcium level. The essential calcium-binding molecule calmodulin Cam1p, which localizes at the SPBs (Moser et al., 1997), is a more likely candidate that regulates the localization of SIN proteins.

Pkd2p exhibits some striking similarities to the growth-promoting MOR pathway, but they showed differences as well. They share a common antagonism towards SIN during cytokinesis. Similar to the *pkd2* mutants, the MOR mutants also prevent the SIN mutant cells from lysis but not as completely. Both localize to the growth zones of the cell tips during interphase and of the division plane during cytokinesis (Hirata et al., 2002; Hou et al., 2003; Verde et al., 1998)). Both MOR and *pkd2* mutants failed to expand their volume fast enough to keep up with the increase of biomass, as demonstrated by a significant increase of intracellular concentration of the constitutively expressed GFP. These similarities suggest that MOR may play a similar role as Pkd2p in regulating the intracellular osmolarity to promote cell growth. This is supported by our observation that the double mutants of MOR and *pkd2* exhibited a more serious defect in temporary deflation, compared to the *pkd2* mutant. There are two key differences between *pkd2* and MOR. Unlike MOR (Das et al., 2009) Pkd2p does not regulate the Cdc42-mediated polarity pathway. Another difference lies in their role in the side growth of fission yeast cells. Such growth is common among the MOR mutant cells, but it is inhibited by *pkd2* mutations. This indicates that the ectopic cell growth depends on *pkd2* but not MOR. Combined, we propose that MOR promotes cell growth through both the Cdc42p mediated cell polarity pathway (Das et al., 2009; Tay et al., 2019) and Pkd2p-regulated intracellular osmolarity.

Genetic screens have identified quite a number of SIN suppressors which include *ace2*, *dnt1*, *scw1*, *sec8*, *ypa1*, *ypa2*, and *zfs1* (Beltraminelli et al., 1999; Goyal and Simanis, 2012; Jin and McCollum, 2003; Jin et al., 2007; Jin et al., 2006; Karagiannis et al., 2002; Ray et al., 2010). They play a variety of molecular functions including exocytosis, RNA binding, and mitotic progression. This suggests that Pkd2p may not be alone in suppressing SIN during cytokinesis through its promotion of cell growth transition.

The role of Pkd2p in the cell size growth during interphase

One of the most striking phenotypes of the *pkd2* mutants is the temporary deflation. Both *pkd2-81KD* and *pkd2-B42* exhibited such a defect (Morris et al., 2019), but it was much more prevalent among the latter at the restrictive temperature. The deflation stalled the already slower than normal expansion of the mutant cells. In fission yeast as in other fungi, maintenance of cell volume depends on the difference between the intracellular and extracellular osmolarity, the

turgor pressure (Lew, 2011; Minc et al., 2009). The temporary deflation phenotype thus suggests that Pkd2p is essential for regulating the homeostasis of the intracellular osmolarity. It is supported by the direct measurement of the stiffness of the *pkd2* mutant cells through AFM. Consistent with a mutant with a defect in intracellular osmolarity, the mutant cells are softer than the wild type. Further, the stiffness was far more heterogeneous among the mutant cells, compared to that of the wild type.

We considered but largely found no evidence to support an alternative model that Pkd2p promotes cell wall biosynthesis. Like other fungi, the fission yeast cell wall is also essential for its growth. However, the cell wall structure of the *pkd2-81KD* mutant cells is similar to that of the wild-type cells (Morris et al., 2019). Unlike most mutants of cell wall biosynthesis, the *pkd2* mutant's viability cannot be fully rescued by supplementing the media with sorbitol. Lastly, while the mutants of cell wall assembly frequently lysed during cell separation (Cortes et al., 2012; Munoz et al., 2013), the *pkd2* mutant cells rarely did so. However, the *pkd2* mutant may still lead to temporary plasma membrane leakage during the deflation. This likely explains why a small fraction of the mutant cells constitutively expressing GFP exhibited significantly lower fluorescence than the average.

We also largely ruled out another alternative model that *pkd2* regulates the Cdc42-mediated polarized cell growth. The ratio of the monopolar to bipolar *pkd2-B42* mutant cells was similar to that of the wild-type. However, it is worth noticing that in almost half of the mutant cells the distribution of the Cdc42 activity indicator CRIB-mCherry was diffuse in the cytoplasm. We consider this a direct result of the temporary deflation, not from a loss of polarized growth. The turnover of Cdc42p molecules may be arrested in these deflated cells, leading to the cytoplasmic localization of this GTPase. This would be similar to those cytoskeletal proteins including actin or tubulin in the deflated cells (Morris et al., 2019). Similarly, the mis-localization of endocytic actin patches in the mutant shall not be attributed to a defect in cell polarity either. Instead, it is more likely due to the reduced membrane stiffness of these mutant cells. This may have facilitated the membrane invagination during endocytosis, resulting in more numerous patches.

The activity of Pkd2p as an ion channel remains unknown. The study of such polycystin channels has been challenging due to our limited knowledge of their activating mechanism. Only

the electrophysiology of mammalian polycystins have been characterized (DeCaen et al., 2013; Delling et al., 2013; Hanaoka et al., 2000). They are calcium-permissive cation channels, but there are continuing debates regarding their activation, molecular composition as well as ion-permeability. In comparison, none of the unicellular polycystin channels including Pkd2p has been characterized for their channel activity yet.

Pkd2p homologues can be found among many fungi species, and they constitute one of seventeen essential fungal protein families (Hsiang and Baillie, 2005). Similar to Pkd2p, Spray of *Neurospora crassa* promotes the tip growth of this filamentous fungus (Bok et al., 2001; Stephenson et al., 2014). It is proposed to regulate the calcium influx and maintain a calcium gradient at the expanding hyphal (Silverman-Gavrila and Lew, 2003). Other Pkd2p homologues included FlcA/B/C of *Aspergillus fumigatus* and CaFlc1-3 of *Candida albicans* (Protchenko et al., 2006). Four homologues of Pkd2p have been identified in *Saccharomyces cerevisiae*, but none of them is essential and their function in cell growth has not been examined (Protchenko et al., 2006; Rigamonti et al., 2015).

In summary, our study reveals the importance of the growth transition during cytokinesis. It is regulated jointly by the polycystin homologue Pkd2p and the yeast Hippo pathway. We propose that this putative TRP channel directly regulates the intracellular osmolarity to promote cell size expansion.

Materials and Methods:

Yeast genetics

Yeast cell culture and genetic procedures were carried out according to the standard methods. We used YE5s media for growing the cells unless specified. SPA5s agar plates were used for genetic crosses and sporulation. A SporePlay+ dissection microscope (Singer, England) was used for tetrad dissection and developing different strains. For viability assays, we inoculated the cells in liquid YE5s media at 25°C overnight before setting up the ten-fold dilution series on YE5S agar plates. The plates were incubated at designated temperatures for two days before being imaged using a photo scanner (Epson).

Identification of temperature-sensitive *pkd2* mutant

To isolate *pkd2* temperature-sensitive mutants, we adopted the approach of marker reconstitution

mutagenesis (Tang et al., 2011) with some modifications. First, we amplified the DNA fragment coding for the C-terminal truncated His5 (His5CterΔ) and *ura4* from the pH5C vector (Tang et al., 2011) by PCR using primers P602 and P603 (Table S3). These primers included nucleotide sequences homologous to the 3′UTR of *pkd2*. The amplified DNA fragment was transformed into yeast using the lithium acetate method. The resulting yeast strain (QCY-999), a Uracil prototroph was selected on EMM plates without uracil supplement and confirmed through PCR and Sanger sequencing. Next, the coding sequence of *pkd2* including its 3′UTR was cloned into the vector pH5D (Tang et al., 2011) which contains the missing DNA coding sequence for the C-terminal fragment of His5 (His5Cter). The resultant vector (QCV-193) was used as the template to perform random mutagenesis of *pkd2* through error-prone PCR. The reaction used for random mutagenesis included Taq DNA polymerase (NEB) in the presence of 200µM $MnCl_2$ (Sigma). The PCR product having the mutated *pkd2* together with the sequence of His5Cter (PCR product) was transformed into the strain (QCY-999) to replace the wild-type gene at its endogenous locus. The transformants were selected on EMM plates without histidine supplement to select for Histidine prototroph. The positive clones were further screened for temperature sensitivity through incubation on YE5s supplemented with Phloxin B at 36°C for two days. The temperature-sensitive mutants were isolated and back-crossed with the wild-type twice to confirm their phenotype. The ORF sequence of the *pkd2-B42* mutant was amplified through PCR and sequenced through the Sangers method to identify the point mutations.

Microscopy

For all microscopy experiments, the cells were inoculated in liquid YE5s media (unless specified) at 25°C for two days before being harvested during the exponential growth phase at a density between 5 x 10^6/ml and 1.0 x 10^7/ml. For temperature-sensitive mutants, exponentially growing cell cultures were temperature shifted for 4 hours (unless mentioned) before live imaging or fixation.

For time-lapse fluorescent microscopy and live cell still microscopy, following temperature shift cells were harvested by centrifugation at 4,000 rpm for 1 minute. Concentrated re-suspended cells were applied to a pad (YE5s + 25% gelatin). The samples were sealed under the coverslip with VALAP (a mix of an equal amount of Vaseline, lanolin, and paraffin) and imaged.

We used a spinning disk confocal microscope equipped with an EM-CCD camera for fluorescence microscopy. The Olympus IX71 microscope was equipped with the objective lenses 100x (NA = 1.40, oil), 60x (NA = 1.40, oil) and 40x (1.30, oil), a confocal spinning disk unit (CSU-X1, Yokogawa, Japan), a motorized XY stage and a Piezo Z Top plate (ASI, USA). Solid-state lasers of 405 nm, 488 nm, or 556 nm were used at a power of no more than 5 mW (< 10%). The images were acquired by an Ixon-897 camera controlled by iQ3.0 (Andor, Ireland). We imaged cells by acquiring 15 slices at a step size of 0.5 µm or 8 slices at a step size of 1 µm for Z-series. Most time-lapse microscopies were done at the room temperature maintained at around 23°C. To minimize the temperature variations, we undertook microscopy of both the wild-type and mutants on the same or consecutive days.

For time-lapse microscopy to measure the tip growth, 20 µL of exponentially growing cell culture was spotted onto a glass coverslip (#1.5) in a 10 mm petri-dish (Cellvis, USA). The coverslip was precoated with 50 µL of 50 µg/mL lectin (Sigma, L2380) which was allowed to dry overnight at 4°C. The cells were overlaid with a 9 mm diameter YE5s agar block (~ 5 mm height), petri-dish was covered, and imaged. To measure the tip growth at the restrictive temperature, time-lapse microscopy was performed using an Olympus IX81 microscope enclosed in a temperature-controlled chamber (Precision Control). Additionally, exponentially growing cells were first temperature shifted in liquid culture at 36°C for 4 hours. Following mounting in petri-dish as above, they were immediately imaged in the pre-equilibrated chamber. Brightfield images were acquired with a 60x oil objective lens (Olympus, NA=1.42) and a CoolSNAP HQ2 camera (Photometrics) with 1 X 1 binning. For measuring growth rate at room temperature, the spinning disk confocal microscope mentioned was used.

To measure the septation or mitotic indices, calcofluor or DAPI stained cells were imaged with an Olympus IX81 microscope equipped with a 60x oil lens (NA=1.42) and a digital camera C11440 (Hamamatsu, Japan). Images were acquired using CellSens (Olympus). Brightfield images were illuminated with a LED lamp.

For visualizing the cell wall or septum, cells were fixed with 4% paraformaldehyde (Fisher), washed with TEMK buffer, and stained cells with 1µg/mL of Calcofluor White stain (Sigma). For nuclear staining, cells were fixed with cold 70% ethanol and stained with 1µg/mL

DAPI (Sigma). For some septation indices measurement, the spinning disk confocal microscope with a 40x oil objective was used. Laser at 405nm was used at 1% with 25 m/s exposure was used in this case.

Image analysis

We used Image J (NIH) to process all the microscopy images, with either freely available or customized macros/plug-ins. For quantitative analysis, the fluorescence micrographs were corrected for both X-Y driftings by StackReg plug-in (Thevenaz et al., 1998) and photo-bleaching by EMBLTools plug-in (Rietdorf, EMBL Heidelberg). Unless specified, the average fluorescence of all the Z-slices were used for quantification. All the measurements were corrected with background subtraction.

The SPB localization of Cdc7p-GFP, Sid2p-GFP, and Mob1p-GFP was quantified by measuring the total fluorescence in a 0.8 µm by 0.8 µm (8 x 8 pixels) circle. The background fluorescence was the fluorescence intensities in a ring of 1µm (12 x 12 pixel) surrounding the circle. The contractile ring localization of Sid2p-GFP and Mob1p-GFP was quantified by measuring the fluorescence in a 3–4µm by 0.8 µm (30–40 x 8 pixels) rectangle centering on the cell division plane. The background fluorescence was the fluorescence intensity in 3–4 µm by 0.2 µm rectangle (30–40 x 2 pixels) adjoined to the division plane on both sides.

All the figures were made on CanvasX (ACD Systems) and the plots were created using Origin (OriginLab) or KaleidaGraph.

Atomic Force Microscopy imaging and analysis of cells

Yeast strains were cultured in YE5S medium at 25°C in the mid-log phase ($OD_{595} < 0.6$) for 36 hours prior to imaging. For restrictive temperature experiments, cells were shifted to 36°C for 8 hours. Cells for AFM imaging and analysis were centrifuged at 500g and washed with EMM5S medium prior to plating on plastic dishes. Plastic dishes were prepared for yeast cell adhesion by plasma cleaning with PDC-32G plasma cleaner (Harrick Plasma, Ithaca, NY) for 3 minutes followed by incubation for 48 hours at 4°C with 0.8 mg/mL CellTak adhesive (Corning Life Sciences, Glendale, AZ) diluted in 0.1M $NaHCO_3$. Dishes were washed twice with ddH_2O to remove excess CellTak prior to plating cells. Yeast cells were added to the dish and centrifuged

at 500g for 20 seconds using a swinging bucket rotor. Non-adherent cells were removed by three EMM5S washes and aspiration.

Topographical height and deflection AFM images were obtained in contact mode using an MFP-3D AFM (Asylum Research, Santa Barbara, CA). Silicon Nitride AFM pyramidal tip PNP-TR probes (Nanoworld, Neuchatel, Switzerland) with a nominal spring constant of 0.32 N/m were used for all experiments. Cells were maintained in EMM5S media throughout AFM imaging and analysis to prevent drying out. 2D images were exported from MFP-3D software and scale bars were added in Adobe Photoshop. Following topographical imaging, force data was obtained from yeast cells at a deflection setpoint of 4nN to minimize damage to the cell surface. Ten representative points were selected along the length of each cell, and ten force curves were obtained at each location, for a total of 100 force curves per cell. The extension force curve representing the tip approach and contact with the surface was used to calculate the spring constant for the surface. The spring constants (k_{cell}) were calculated from the linear region of the extension curve using a two-spring model with the equation:

$$\frac{1}{k_{effective}} = \frac{1}{k_{cell}} + \frac{1}{k_{cantilever}}$$

where $k_{cantilever}$ was experimentally calculated using the thermal tuning method (Hutter and Bechhoefer, 1993), and the slope of the extension force curve linear region is $k_{effective}$ (Volle et al., 2008). Data processing was performed through MFP-3D software in Igor Pro to obtain curve fits and spring constants.

Acknowledgement

QC conceptualized the study, DS, JG, and QC designed the experiments, DS, DI, EG, MC, JG, and QC carried out the experiments, DS, DI, EG, MC, JG, and QC analyzed the data, DS, JG, and QC wrote the manuscript. The authors thank Abhishek Poddar and Mamata Malla for their technical support. The authors thank Mohan Balasubramanian (University of Warwick, UK), Daniel McCollum (University of Massachusetts Medical School), Jian-Qiu Wu (Ohio State University), and Pilar Perez (University of Salamanca, Spain) for sharing yeast strains and plasmids with us. We acknowledge the National BioResources Project —Yeast Base (Japan) for sending yeast strains. We would like to thank the group of Song-Tao Liu for sharing their microscope.

The authors declare no competing interests.

This work has been supported by the University of Toledo startup fund (QC), National Institutes of Health grant R15GM134496 (QC), DeArce-Koch Memorial Fund (QC), University of Toledo Undergraduate Summer Research and Creative Activities Program (DI), Wellesley College startup fund (JG), and National Science Foundation grant DBI1528288 (JG). The content is solely the responsibility of the authors and does not necessarily represent the official views of the National Institutes of Health.

Figures and Figure legends:

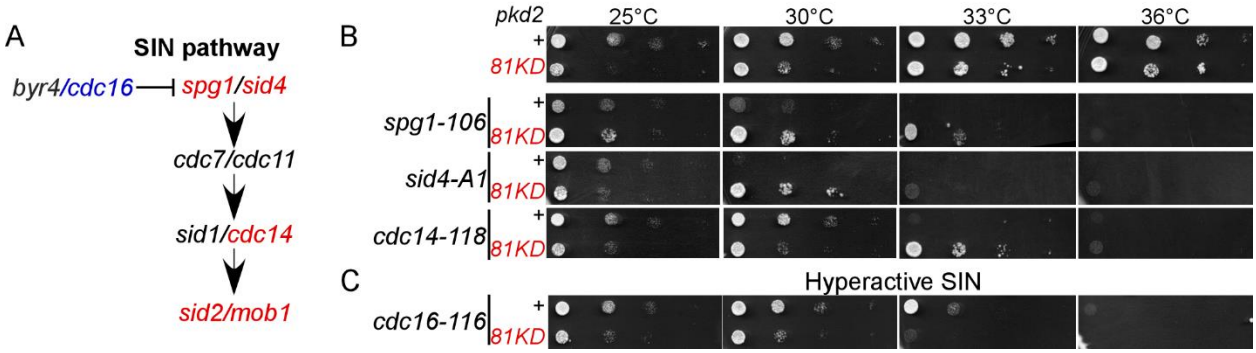

Figure 1. Epistatic genetic interactions between *pkd2-81KD* and SIN.

(A) Schematic of the SIN pathway. The genes whose mutants have been tested are colored in either blue (negative interaction) or red (positive interaction)

(B–C) Ten-fold dilution series of fission yeast strains at the indicated temperatures. The data are representatives from at least two independent biological repeats.

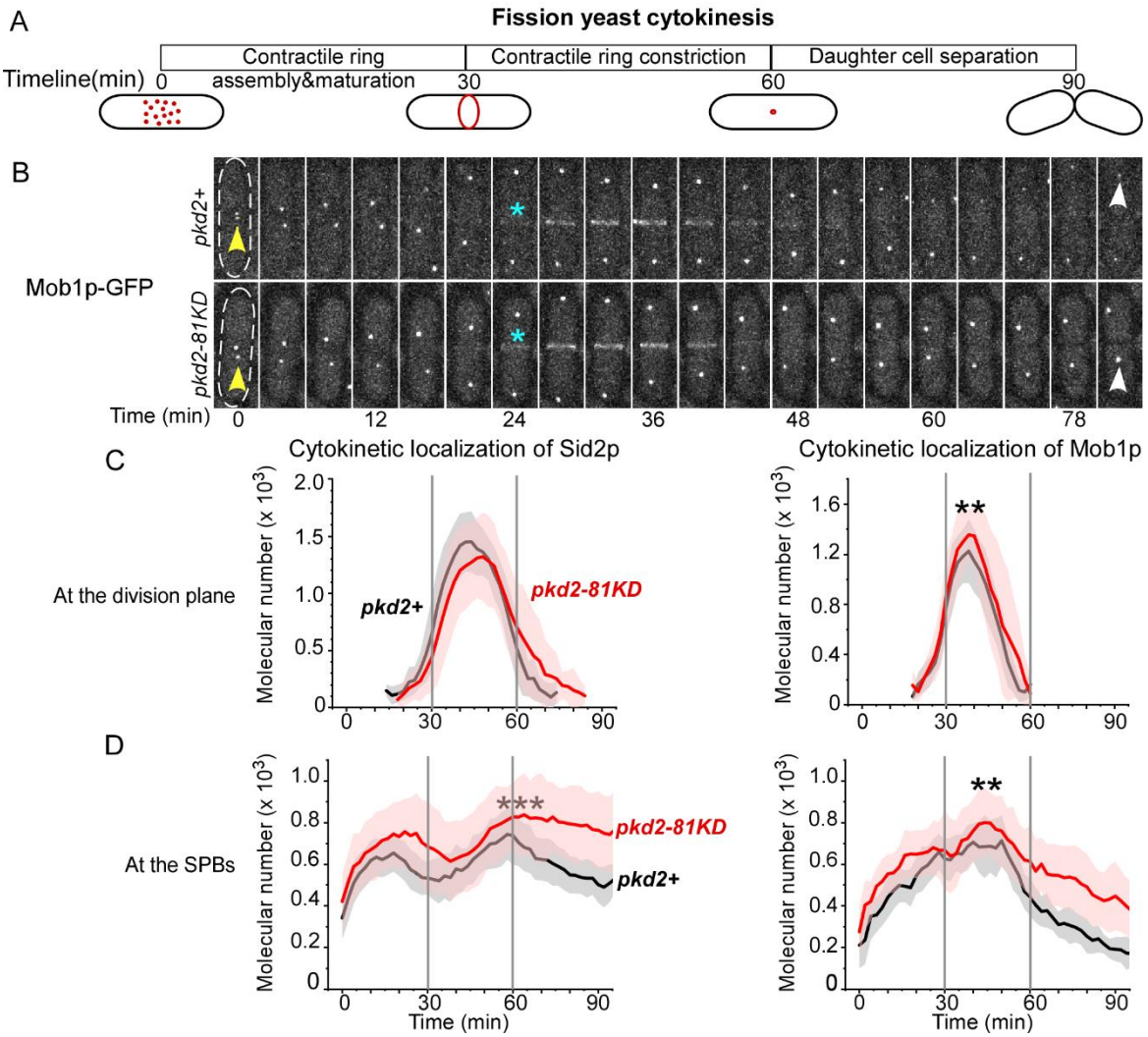

Figure 2. Localization of SIN proteins in *pkd2-81KD* cells during cytokinesis.

(A) Schematic of fission yeast cytokinesis. Shown is the average timeline of the wild-type cells. Time zero denotes the separation of SPBs during prometaphase.

(B) Time-lapse micrographs of either a wild-type (top) or a *pkd2-81KD* (bottom) cell expressing Mob1p-GFP. Number denotes time in minute after SPB separation. Interval = 4minutes. Arrowheads: SPB. Asterisk: Appearance of Mob1p-GFP at the division plane.

(C–D) Average time-courses of the number of Sid2p-GFP (left) or Mob1p-GFP (right) molecules in the division plane (C) or SPBs (D) of either wild-type (black line) or the *pkd2-81KD* cells (red line). The data was pooled from two independent biological repeats (n>20). The peak number of molecules were used for statistical tests. **: $P < 0.01$, ***: $P < 0.001$.

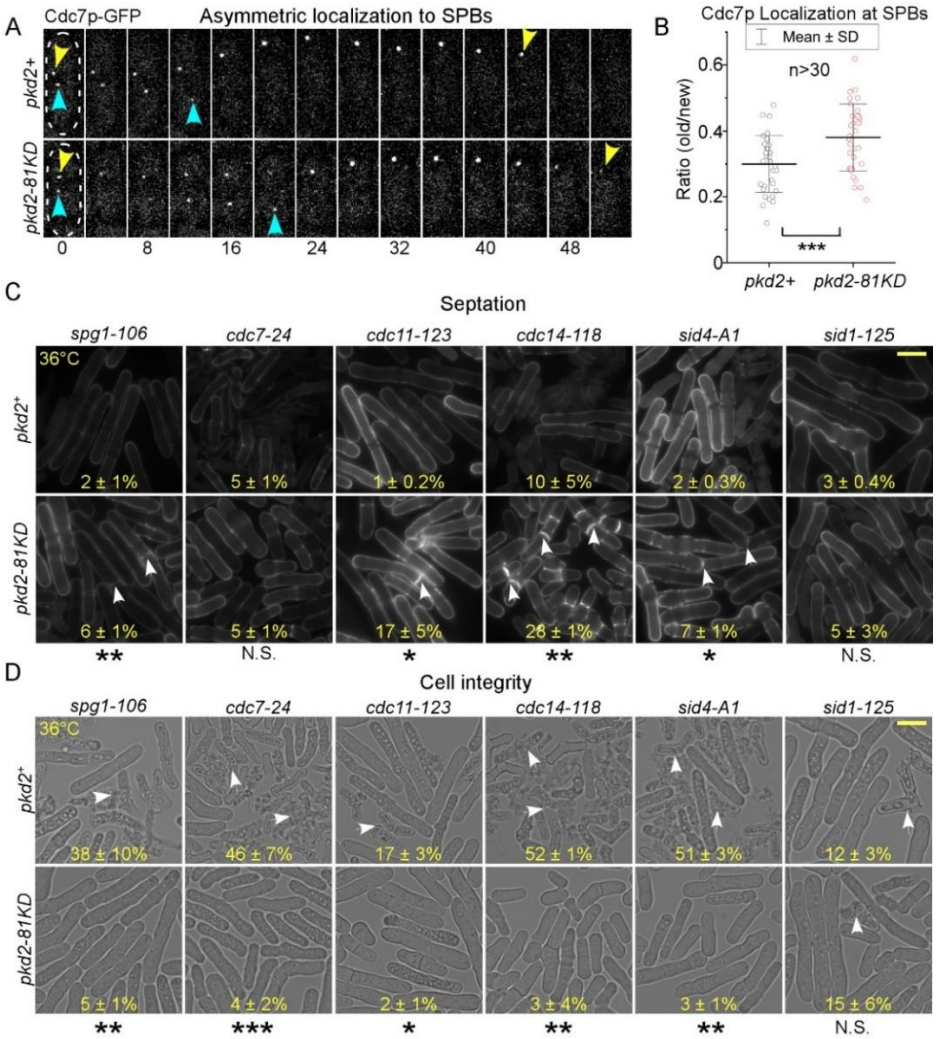

Figure 3. Activities of SIN in *pkd2-81KD* cells.

(A–B) Asymmetric distribution of Cdc7p-GFP at two SPBs during cell division. (A) Time-lapse micrographs of either a wild-type (top) or a *pkd2-81KD* (bottom) expressing Cdc7p-GFP. Number represents time in min after the SPB separation. Arrowheads: new (yellow) or old (blue) SPB. (B) Dot plots of ratio (old:new) of the dwelling time of Cdc7p-GFP at the two SPBs (n > 30). The data was pooled from two independent biological repeats.

(C–D) Micrographs of SIN (top) and *pkd2-81KD* SIN (bottom) mutants fixed at the restrictive temperature of 36°C. **(C)** The cells stained with calcofluor. Arrowhead: septated cell. **(D)** Bright-field images. Arrowhead: lysed cell. The percentages of either septated (C) or lysed cells (D) (average ± standard deviation) are noted. The data was pooled from at least two independent biological repeats (n > 400). Bar represents 10µm. *:P<0.05, **:P<0.01, ***: P<0.001.

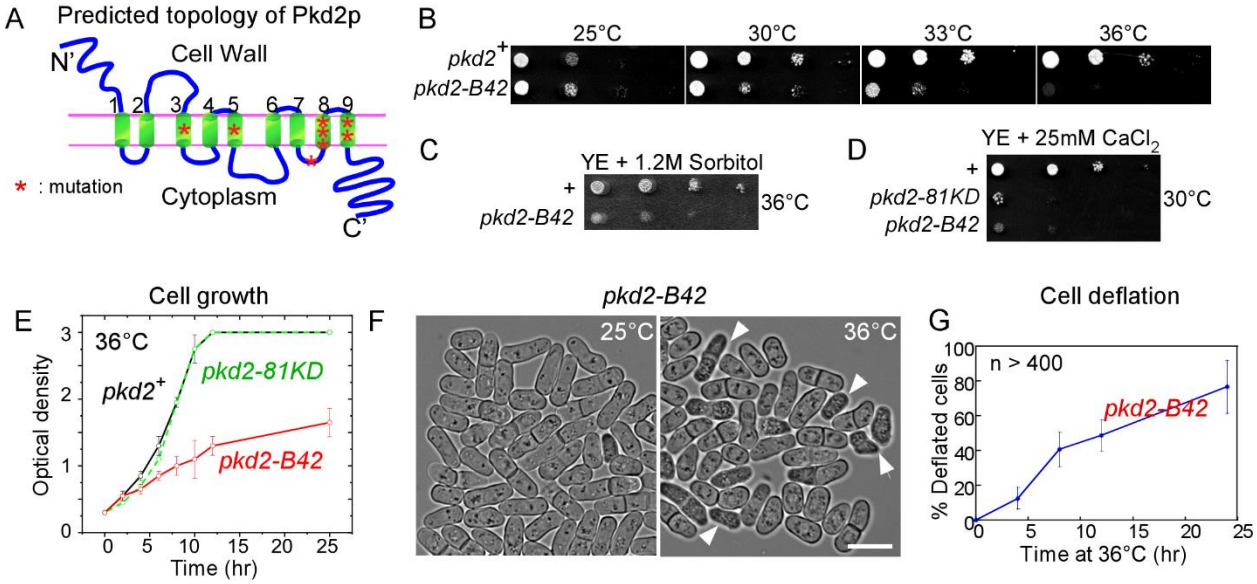

Figure 4. A novel temperature-sensitive mutant *pkd2-B42*.

(A) Schematic of the predicted topology of the wild-type Pkd2p. The mutated residues in *pkd2-B42* are shown in red asterisks. Numbers denote the nine transmembrane helices.

(B–D) Ten-fold dilution series of the yeast strains at indicated temperatures and conditions.

(E) Growth curve of the wild-type (black line), *pkd2-81KD* (green) and *pkd2-B42* (red) cells at 36°C. Error bars represent standard deviations.

(F) Bright-field micrographs of *pkd2-B42* cells at either 25°C (left) or 36°C (right). Bar represents 10µm.

(G) Time course of the percentage of deflated *pkd2-B42* cells at 36°C. Data was pooled from at least two independent biological repeats. Error bars represent standard deviations.

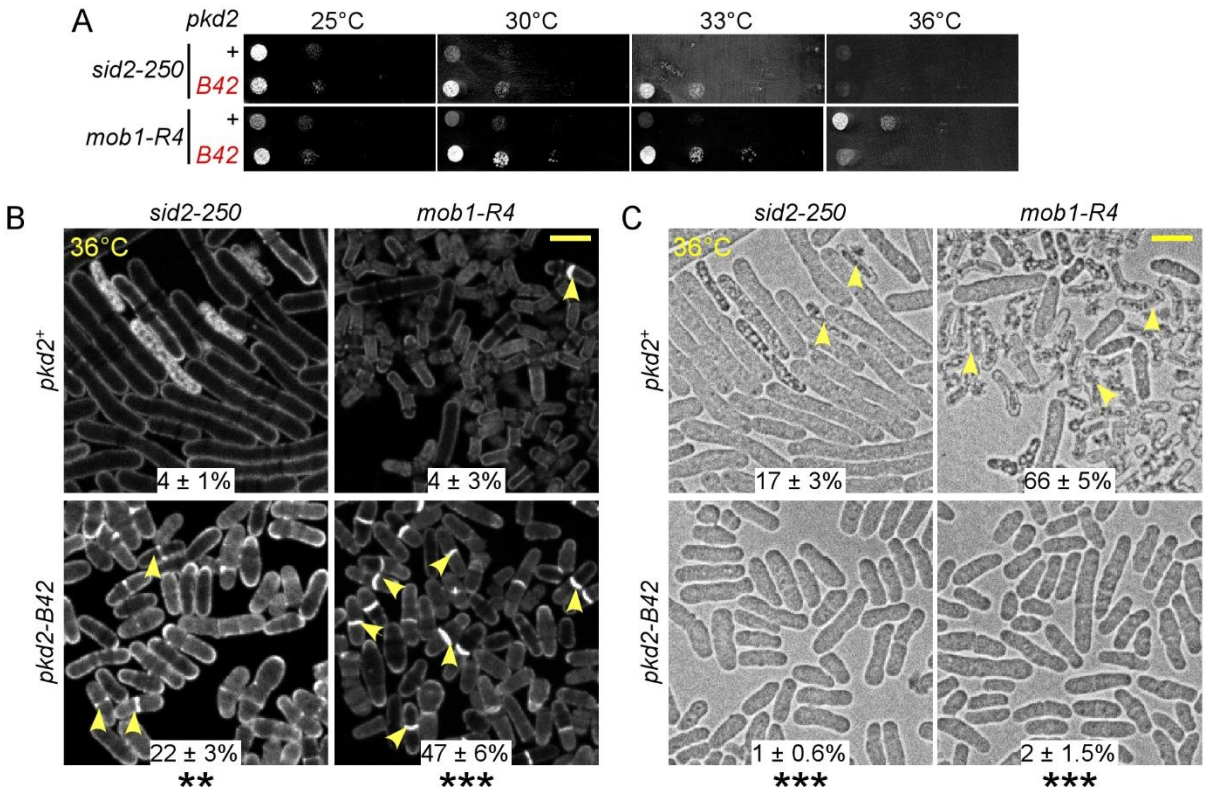

Figure 5. Genetic interaction between *pkd2-B42* and SIN mutants.

(A) Ten-fold dilution series of yeast cells at indicated temperatures.

(B-C) Micrographs of either SIN (top) or *pkd2-B42* SIN (bottom) mutants fixed at the restrictive temperature of 36°C. **(B)** The cells were stained with calcofluor. **(C)** Bright-field micrographs. The percentage of septated (B) or lysed (C) cells are provided (average ± standard deviations). Arrowhead: septated (B) or lysed (C) cells. Data was pooled from three independent biological repeats (n > 500). Bar represents 10µm. **:P<0.01, ***:P<0.001.

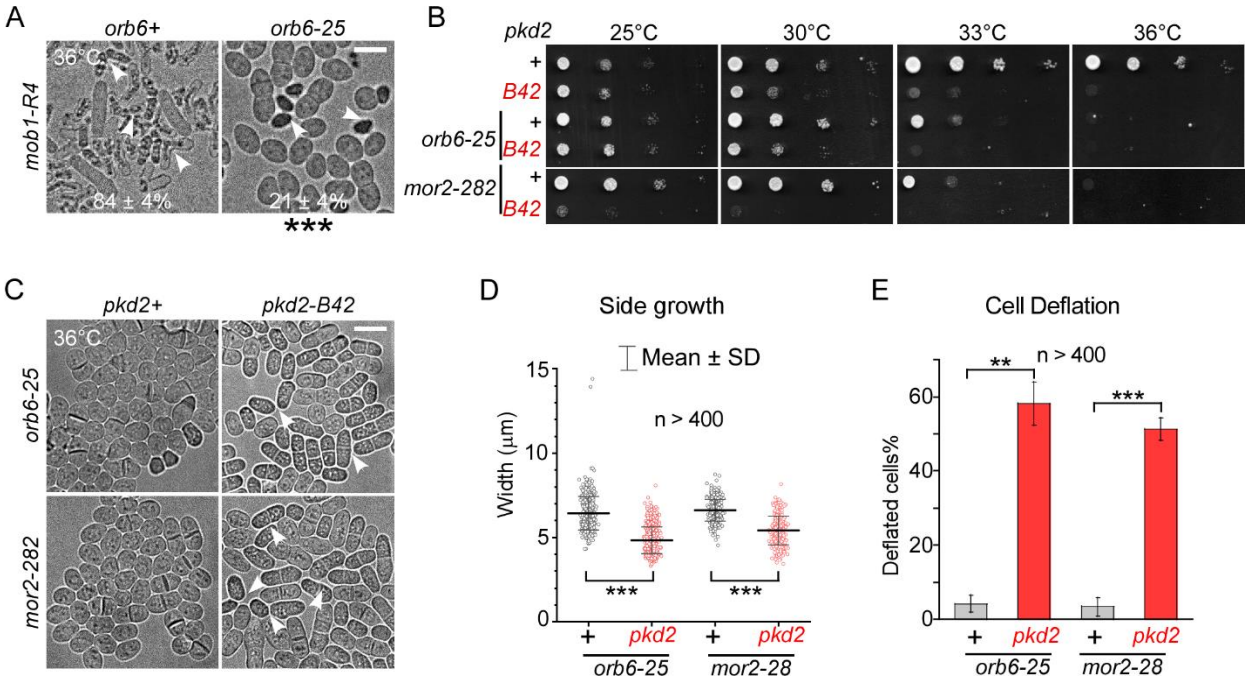

Figure 6. Pkd2p synergizes with MOR pathway in promoting cell growth.

(A) Micrograph of the yeast cells at the restrictive temperature. Number is the percentage of lysed cells (average ± standard deviations). n > 400.

(B) Ten-fold dilution series of yeast at indicated temperatures.

(C–E) Morphological defects of *pkd2-B42 MOR* mutant cells. **(C)** Micrograph of the mutants at 36°C. Arrowhead: deflated cells. **(D)** Dot plot of the width of the mutants. **(E)** Bar graph of the fraction of deflated cells. The data is pooled from two independent biological repeats. Scale bar 10µm. **:P<0.01, ***:P<0.001.

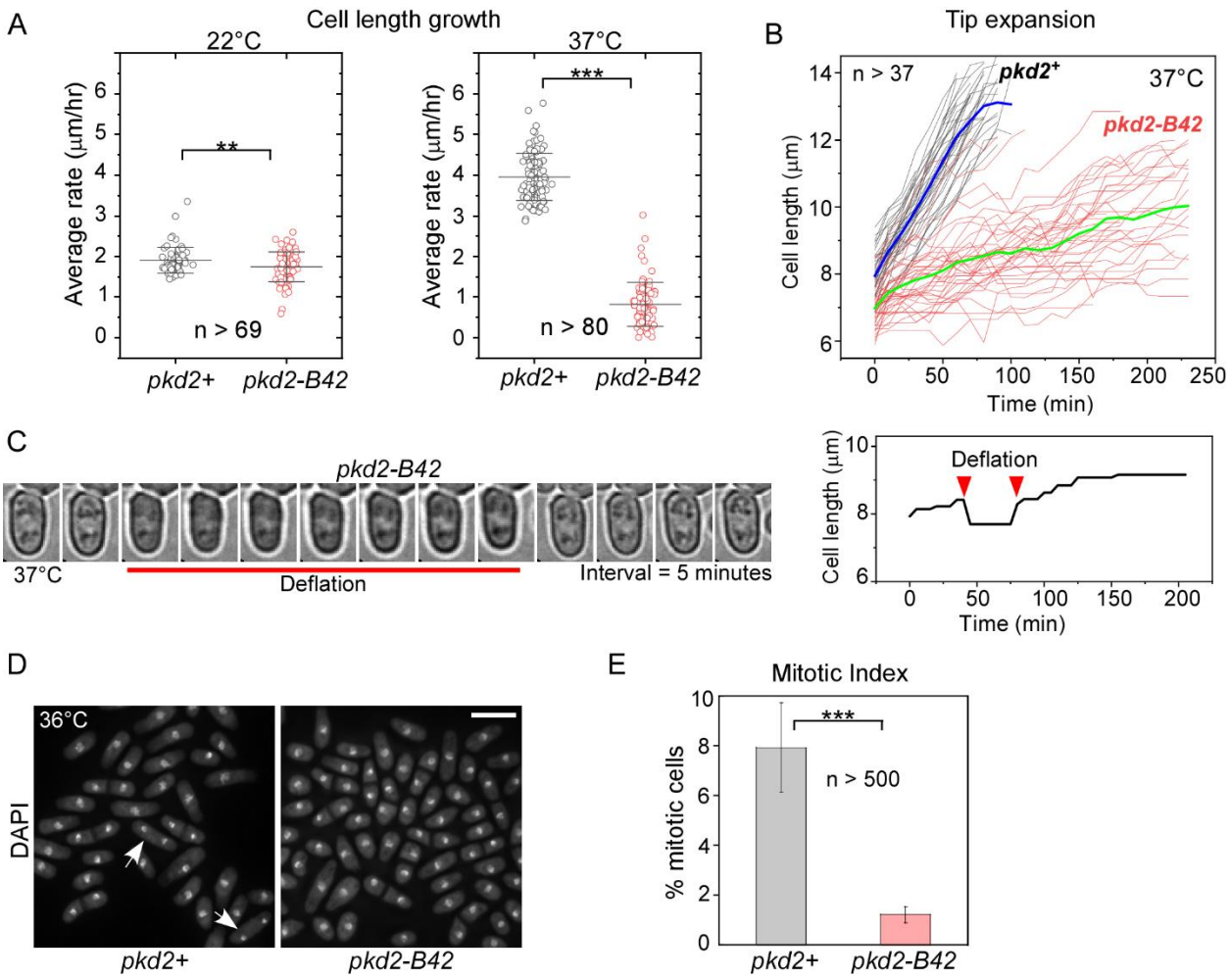

Figure 7. Pkd2p is required for the cell size expansion during interphase growth.

(A–B) Tip expansion of *pkd2-B42* cells. **(A)** Dot plots of the average tip growth rate of the wild-type and the *pkd2* mutant cells at either 22°C or 37°C. Lines represent average ± standard deviations. **(B)** Time courses of the length of individual wild-type (black lines) and *pkd2-B42* cells (red lines) at 37°C. Thick lines (blue: wild type, green: *pkd2-B42*) represent the average time courses.

(C) Temporary growth pauses of a *pkd2-B42* cell at 37°C. Left: Time-lapse micrographs. Right: Time course of the cell length.

(D-E) Fraction of mitotic cells. **(D)** Fluorescence micrographs of either wild-type (left) and *pkd2-B42* (right) cells fixed and stained with DAPI. **(E)** Bar graphs showing the mitotic indices of wild-type and *pkd2-B42* cells. Data were pooled from at least two independent biological repeats. Bar represents 10µm. **:P<0.01 ***: P < 0.001.

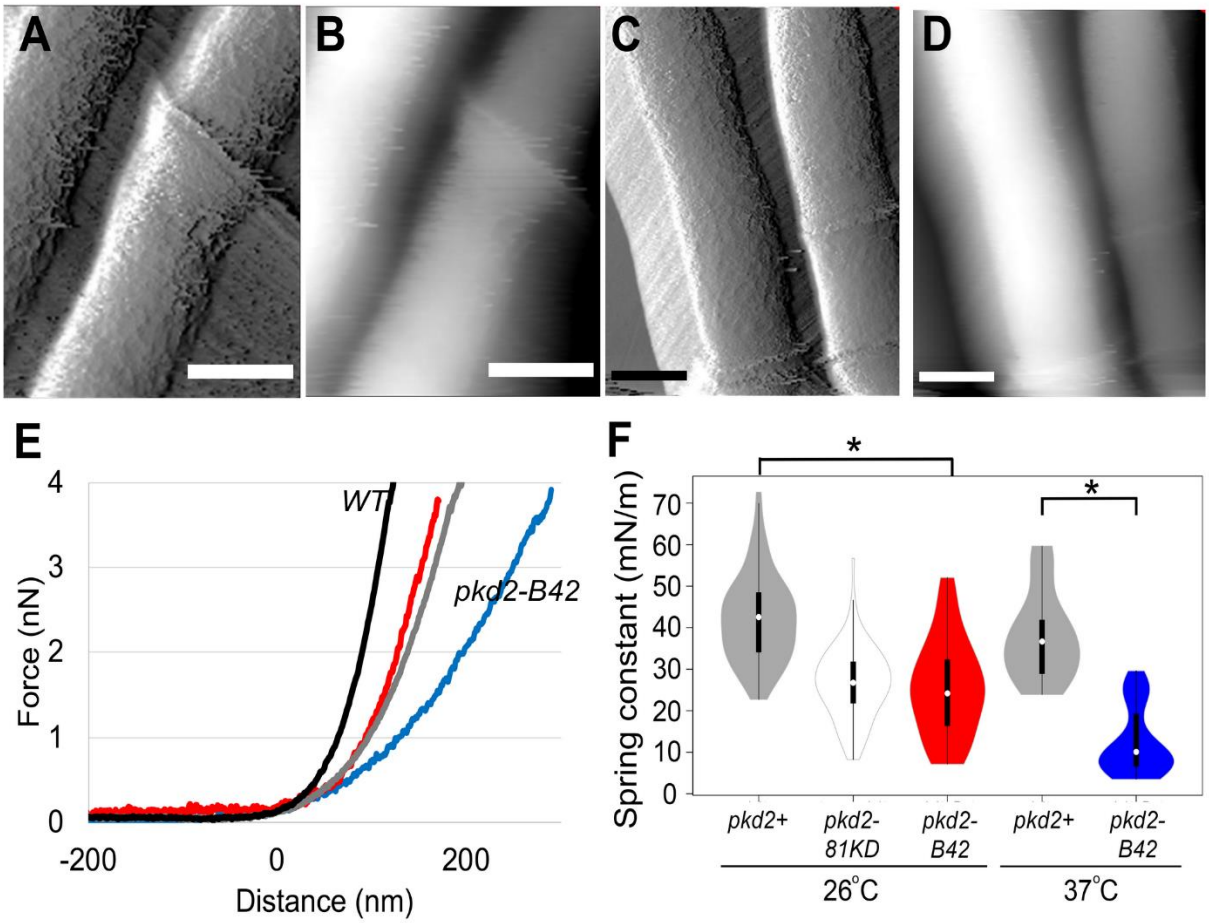

Figure 8. Cellular stiffness is decreased in *pkd2* mutant cells.

(A-D) Atomic Force Microscope (AFM) deflection (A, C) and height (B, D) images of wild-type (A, B) or *pkd2-B42* (C, D) cells acquired by intermittent contact imaging mode. Bars represent 2µm.

(E) Representative extension force curves of the wild-type (black), *pkd2-81KD* (grey), or *pkd2-B42* (red, 26°C) cell surface, or *pkd2-B42* (blue, 37°C). The horizontal linear region of each curve (-200 nm to 0 nm) reflects the cantilever approaching the surface with the zero point along the X-axis indicating the point of contact between the tip and surface. The linear deflection of the cantilever tip occurs as the cantilever tip pushes against the cell wall, which indicates the surface stiffness.

(F) Violin plot of cellular spring constants calculated from extension force curves wild-type (black), *pkd2-81KD* (grey), or *pkd2-B42* (red) cells, at either 26°C or 37°C. The boxed region indicates the upper and lower quartiles for each data set; median is indicated by the horizontal line within the box; whiskers extend to the high and low data points. ($n > 500$, force measurements total from 5 cells per condition). Asterisks indicate $p < 1e^{-5}$, measured by ANOVA and student t-tests.

Supplemental materials:

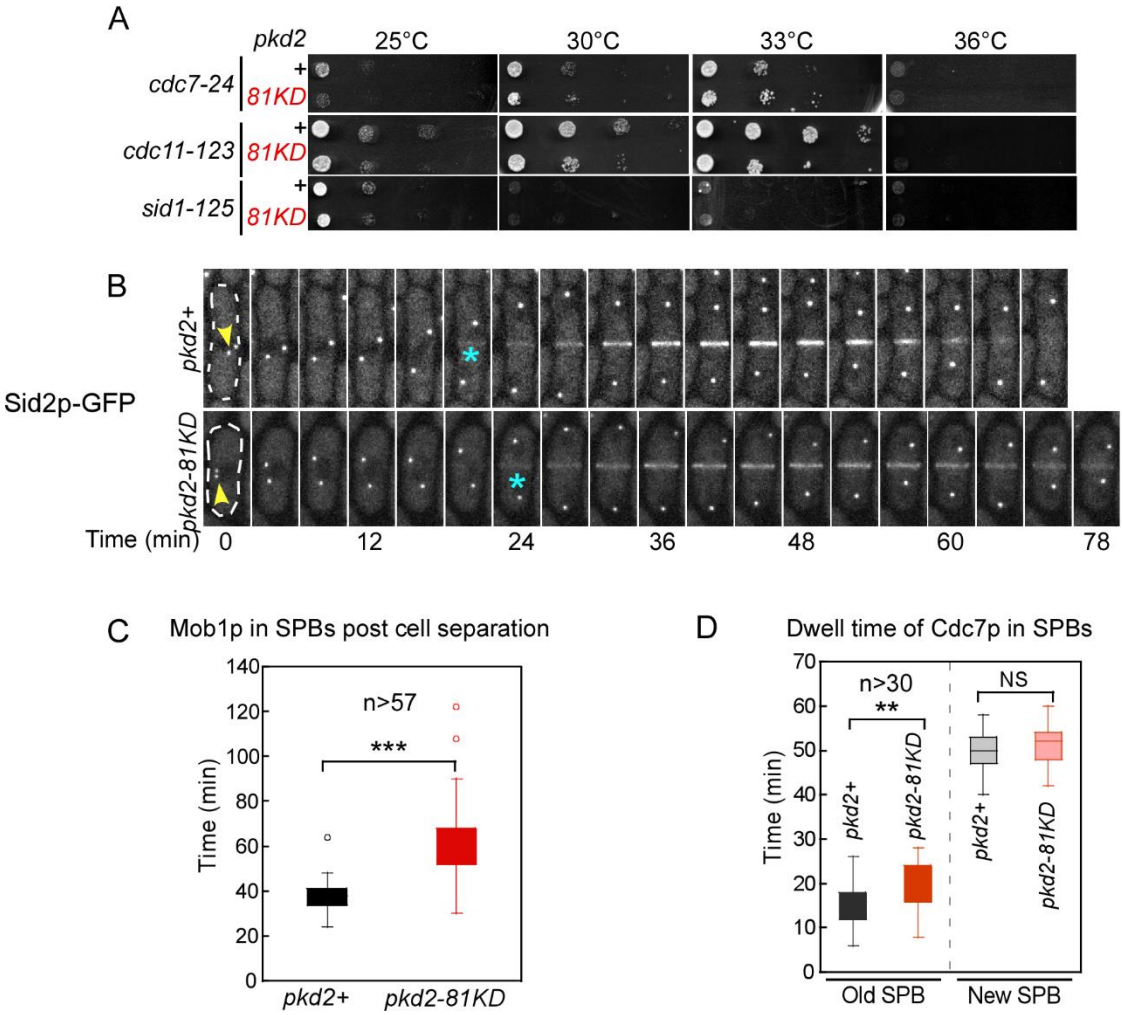

Supplemental Figure S1. Antagonistic relationship between *pkd2* and SIN. Related to Figure 1, 2 and 3.

(A) Ten-fold dilution series of yeast.

(B) Time-lapse micrographs of either a wild-type (top) or a *pkd2* mutant (bottom) cell expressing Sid2p-GFP. Number represents time in minute after the SPB separation. Arrowhead: SPB. Asterisk: appearance of Sid2p-GFP at the division plane.

(C) Box plot showing the dwelling time of Mob1p-GFP at the SPB in the wild-type and *pkd2-81KD* cells, after the cell separation. n>57.

(D) Box plot showing the dwelling time of Cdc7p-GFP at the old and new SPBs in the wild-type and *pkd2*-mutant cells (n > 30). The data is pooled from two biological repeats. **: P<0.01, ***:P<0.001

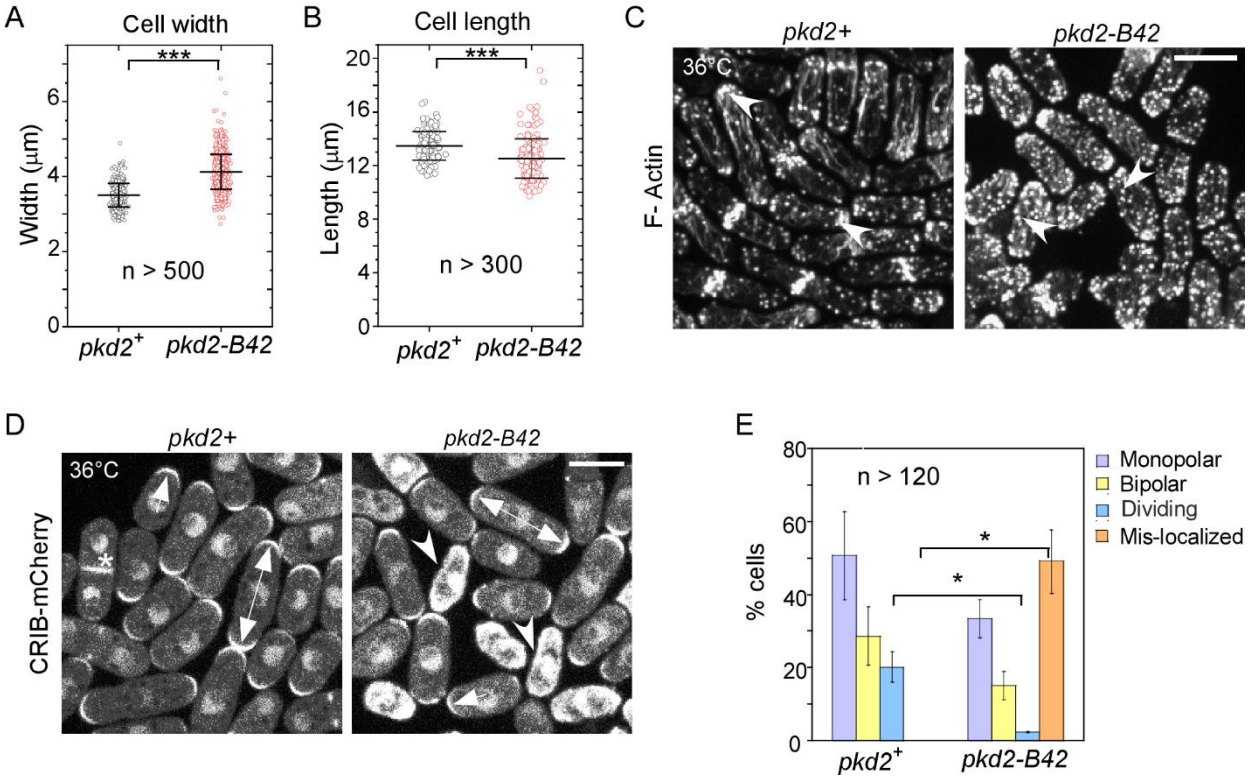

Supplemental Figure S2. Characterization of the temperature-sensitive mutant *pkd2-B42*. Related to Figure 4.

(A–B) Dot plots of the width (A) and length (B) of *pkd2-B42* cells, compared to the wild-type (*pkd2*$^{+}$).

(C) Fluorescent micrograph of fixed and bodipy-phallacidin stained wild-type and *pkd2-B42* cells to visualize actin filaments.

(D–E) The polarity of pkd2-B42 cells. **(D)** Fluorescent micrograph of wild-type and *pkd2-B42* cells expressing the active Cdc42p indicator CRIB-mCherry at 36°C. Single-headed arrow: monopolar cell. Double-headed arrow: bipolar cell. Asterisk: dividing cell. Arrowhead: cell with mis-localized CRIB-mCherry. **(E)** Bar graph showing fractions of the wild-type and *pkd2-B42* cells categorized based on the intracellular localization of CRIB-mCherry. The data is pooled from two biological repeats. Bar represents 10µm. *: P<0.05, ***: P < 0.001

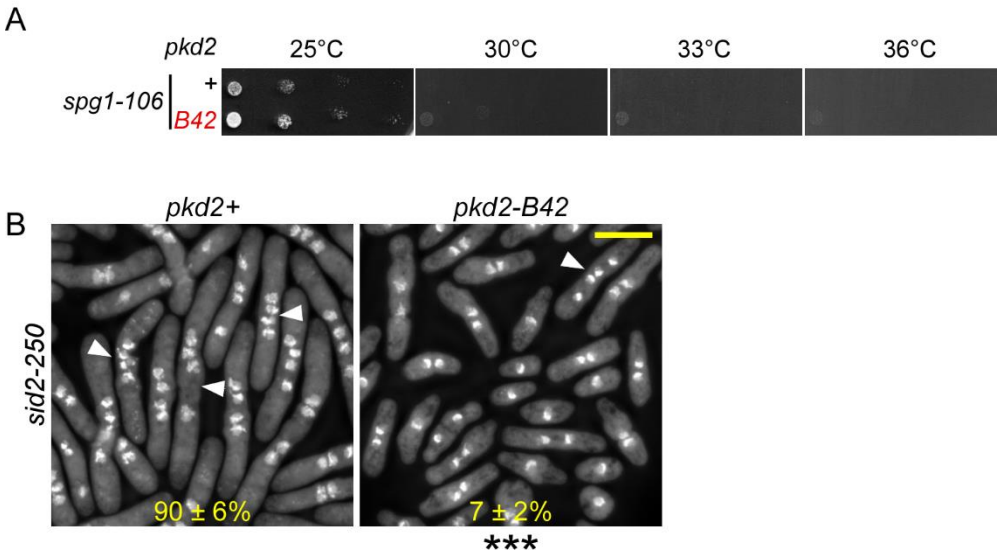

Supplemental Figure S3. Genetic interaction between *pkd2-B42* and SIN mutants. Related to Figure 5.

(A) Ten-fold dilution series of yeast at indicated temperatures.

(B) Fluorescence micrographs of *sid2-250* (left) and *pkd2-B42 sid2-250* (right) cells fixed and stained with DAPI to visualize the nuclei. Arrowhead: cell with 4 nuclei. Numbers represent the percentage of multinucleated cells (average ± standard deviations). n > 400. The data was pooled from at least two independent biological repeats. Bar represents 10µm. ***:P<0.001.

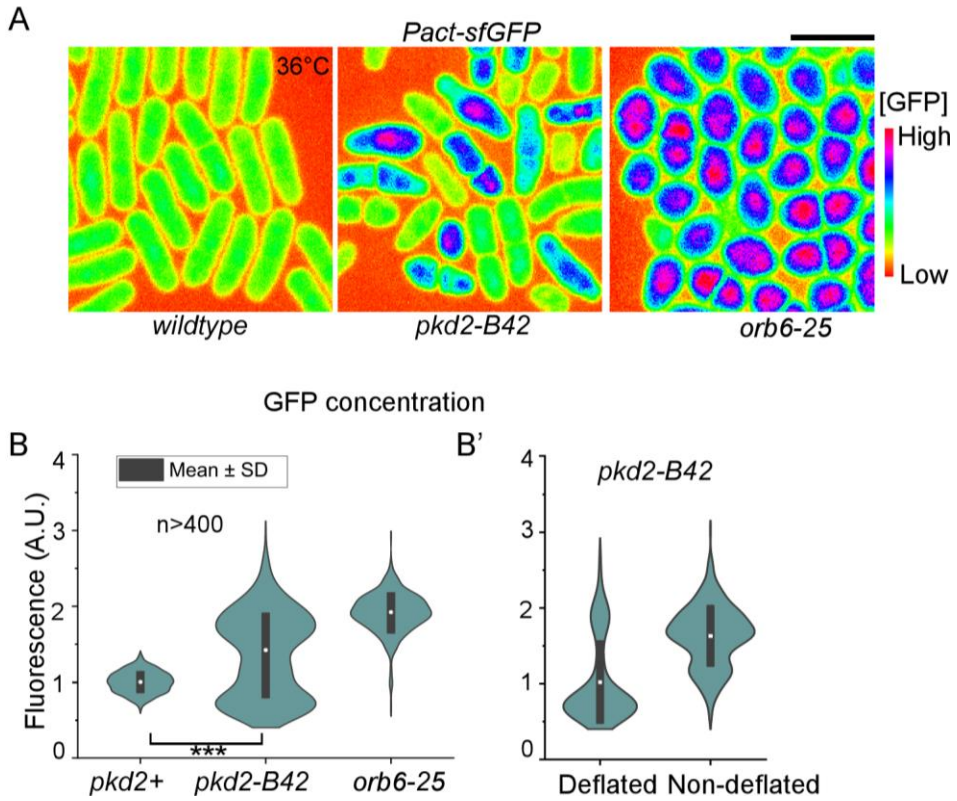

Supplemental Figure S4. Volume expansion of *pkd2-B42* and MOR mutant cells. Related Figure 7.

(A) Fluorescence micrographs (spectrum-colored) of the wild-type (left), *pkd2-B42* (middle) and *orb6-25* (right) cells at 36°C. All of them constitutively expressed sfGFP as a fluorescence indicator of cell volume.

(B) Violin plots of intracellular GFP fluorescence. (B') Violin plots showing the intracellular GFP fluorescence in the deflated and non-deflated *pkd2-B42* cells. n>400. The data were pooled from at two independent biological repeats. Bar represents 10µm. ***: $P < 0.001$.

Supplemental movies:

Supplemental movie S1: Tip growth of the wild type. Time-lapse of a wild-type cell at 37°C during interphase growth. Number represents time in minute after cell separation.

Supplemental movie S2: Tip growth of *pkd2-B42*. Time-lapse of a *pkd2-B42* cell at 37°C during interphase growth. Number represents time in minute after cell separation. *pkd2-B42* cell expands at an average rate of 0.8µm/hour at this temperature.

Supplemental movie S3: Temporary deflation and tip growth pause of *pkd2-B42*. Time-lapse of *pkd2-B42* cells at 37°C during interphase growth. Arrows point to the deflating cells. Number represents time in minute.

Table S1: Genetic interactions between *pkd2-81KD* and other cytokinetic mutants

Gene	Mutant	Genetic interactions
ace2	*ace2Δ*	-
agn1	*agn1Δ*	*No*
ags1	*mok1-664*	*No*
bgs4	*cwg1-2*	*No*
cdc11	*cdc11-123*	*No*
cdc14	*cdc14-118*	++
cdc16	*cdc16-116*	--
cdc42	*cdc42-1625*	*No*
cdc7	*cdc7-24*	*No*
eng1	*eng1Δ*	*No*
exo70	*exo70Δ*	-
far8	*far8Δ*	*No*
mid1	*mid1Δ*	*No*
mid2	*mid2Δ*	*No*
mor2	*mor-282*	--
myp2	*myp2Δ*	*No*
orb6	*orb6-25*	--
rga7	*rga7Δ*	*No*
rgf1	*rgf1Δ*	*No*
rgf2	*rgf2Δ*	*No*
sid1	*sid1-125*	*No*
sid4	*sid4-A1*	+
spg1	*spg1-106*	++
sty1	*sty1Δ*	*No*

"++" or "+": strong or weak positive interactions. "--" or "- ": strong or weak negative interactions. No: no interactions. Genetic interactions with the other 11 cytokinesis mutants were published in an earlier study (Morris et al., 2019).

Table S2: List of all mutations in *pkd2-B42*

Residue	Position in the transmembrane helices	Mutation	Amino acid change
335	3rd	F → S	Hydrophobic to Polar
408	5th	S → P	Polar to Polar
521	Between 7th and 8th	N → D	Polar to Polar
530	8th	M → V	Hydrophobic to Hydrophobic
534	8th	S → G	Polar to Polar
543	8th	Q → E	Polar to Charged
555	9th	I → T	Hydrophobic to Polar
571	9th	I → T	Hydrophobic to Polar

Table S3: List of primers used in the development of *pkd2-B42*

Number	Sequence
QC-P596	*AGAGTCGAATTTTATTGATG*
QC-P597	*ATGCCGCATAGTTAAGCCAG*
QC-P598	*GTCGTTCTTTTCCTGACATA*
QC-P599	*TATGTCAGGAAAAGAACGAC*
QC-P600	*CTGAAGTCCCAAGCACGAAG*
QC-P601	*CTTCGTGCTTGGGACTTCAG*
QC-P602	*ACGTTTATTAACATTTTATTGAAACAATCTATAGACACCGGTAAGAATAAATCCATAAGCCATTCCCAAA-GGAAATAGTAAGGCTAGTAG*
QC-P603	*GAATATATGCCTATTCGCAATCTAGAATTCCTTTGAATACACCCAATTACAAGCTTAAACGATTCGGTAT-TAAAAATAGGCGTATCACGAGG*
QC-P604	*AGCATATTTGTTGGATGTGC*
QC-P605	*AA-CGATCG-ATGAGGCTTTGGAGAAGCCCAC*
QC-P606	*AA-GGATCC-TTTGGGAATGGCTTATGGATTTATTC*
QC-P607	*GACGAAGCTCTTTCTAGAAGCGTAGT*

675 **Table S4: List of yeast strains used in this study**

Strains number	mating type	Genotype	Source
FY13846	*h-*	*cps212-282 or mor2-282*	(CP28-2) NBRP Japan
FY38515	*h-*	*his5+:pact1:CRIB[gic2aa1-181]-3mCherry:bsdMX*	(AV2324) NBRP Japan
FY527	*h-*	*leu1-32 ura4-D18 his3-D1 ade6-M216*	Lab stock
FY528	*h+*	*leu1-32 ura4-D18 his3-D1 ade6-M210*	Lab stock
JW7551	*h?*	*cwg1-2*	Jian Wu
JW7572	*h-*	*mok1-664*	Jian Wu
MBY2415	*h+*	*cdc7-GFP::ura4*	Mohan Balasubramanian
MBY6218	*h-*	*ade5D ade7::Ade5 his5D leu1-32 ura4D-18*	Mohan Balasubramanian
PPG5660	*h+*	*leu1-32 ura4-D18 cdc42-1425:kanMX6*	Pilar Perez
QC-Y569	*h-*	*cdc11-123*	Lab stock
QC-Y570	*h-*	*sid4-A1*	Lab stock
QC-Y571	*h+*	*spg1-106*	Lab stock
QC-Y573	*h+*	*cdc16-116*	Lab stock
QC-Y574	*h-*	*cdc7-24*	Lab stock
QC-Y576	*h+*	*sid2-250*	Lab stock
QC-Y577	*h-*	*mob1-R4*	Lab stock
QC-Y624	*h+*	*cdc14-118*	Lab stock
QC-Y670	*h-*	*myp2::kanMX6*	Lab stock
QC-Y675	*h-*	*mob1-mEGFP-kanMX6*	Lab stock
QC-Y676	*h-*	*sid2-mEGFP-kanMX6*	Lab stock
QC-Y723	*h+*	*sid1-125 ura4-D18 leu1-32 ade6-210*	Lab stock
QC-Y725	*h+*	*ace2::kanR ura4-D18 ade6-216 leu1-32 h+*	Lab stock
QC-Y743	*h+*	*far8::kanMX6*	Bioneer
QC-Y803	*h-*	*orb6-25*	Lab stock
QC-Y810	*h-*	*KanMX6-P81nmt1-pkd2 leu1-32 ura4-D18 his3-D1*	Lab stock
QC-Y817	*h+*	*kanMX6-81xnmt1-pkd2 leu1-32 ura4-D18 his3-D1 ade6-M?*	Lab stock
QC-Y874	*h-*	*sty1::kanMX6*	Lab stock
QC-Y930	*h?*	*kanMX6-81xnmt1-Pkd2 sid2-mEGFP-kanMX6*	This study
QC-Y933	*h?*	*kanMX6-81xnmt1-Pkd2 mob1-mEGFP-kanMX6*	This study
QC-Y976	*h?*	*kanMX6-81xnmt1-pkd2 cdc16-116*	This study
QC-Y977	*h?*	*kanMX6-81xnmt1-pkd2 cdc14-118*	This study
QC-Y978	*h?*	*kanMX6-81xnmt1-pkd2 cdc11-123*	This study
QC-Y979	*h?*	*kanMX6-81xnmt1-pkd2 spg1-106*	This study
QC-Y980	*h?*	*kanMX6-81xnmt1-pkd2 sid4-A1*	This study
QC-Y983	*h?*	*kanMX6-81xnmt1-pkd2 cdc7-24*	This study
QC-Y999	*h-*	*pkd2-3'UTR-his5CterD-ura4*	This study
QC-Y1010	*h+*	*mid1::kanMX6*	Bioneer
QC-Y1011	*h+*	*mid2::kanMX6*	Bioneer
QC-Y1012	*h+*	*rga7::kanMX6*	Bioneer

QC-Y1013	*h+*	*rgf1::kanMX6*	Bioneer
QC-Y1017	*h?*	*kanMX6-81xnmt1-pkd2 myp2::kanMX6*	This study
QC-Y1017	*h?*	*kanMX6-81xnmt1-pkd2 myp2::kanMX6*	This study
QC-Y1022	*h?*	*kanMX6-81xnmt1-pkd2 mid1::kanMX6*	This study
QC-Y1023	*h?*	*kanMX6-81xnmt1-pkd2 mid2::kanMX6*	This study
QC-Y1024	*h?*	*kanMX6-81xnmt1-pkd2 rga7::kanMX6*	This study
QC-Y1025	*h?*	*kanMX6-81xnmt1-pkd2 rgf1::kanMX6*	This study
QC-Y1031	*h-*	*pkd2::pkd2-B42-ura4+-his5+ leu1-32*	This study
QC-Y1032	*h+*	*pkd2::pkd2-B42-ura4+-hist5+ leu1-32*	This study
QC-Y1032	*h+*	*pkd2::pkd2-B42-ura4+-hist5+ leu1-32*	This study
QC-Y1036	*h?*	*pkd2::pkd2-B42-ura4+-his5+ leu1-32 sid2-250*	This study
QC-Y1037	*h?*	*pkd2::pkd2-B42-ura4+-his5+ leu1-32 mob1-R4*	This study
QC-Y1061	*h+*	*eng1:: KanMx6*	Bioneer
QC-Y1062	*h+*	*rgf2::kanMX6*	Bioneer
QC-Y1070	*h-*	*ura4::Pact-sfGFfP-ura4*	This study
QC-Y1072	*h?*	*pkd2::pkd2-B42-ura4+-his5+ leu1-32 far8::kanMX6*	This study
QC-Y1073	*h?*	*kanMX6-81xnmt1-pkd2 far8::kanMX6*	This study
QC-Y1080	*h?*	*pkd2::kanMX6-81xnmt1-pkd2 ura4::Pact-sfGFfP-ura4*	This study
QC-Y1081	*h?*	*eng1:: KanMx6 pkd2::pkd2-B42-ura4+-his5+ leu1-32*	This study
QC-Y1082	*h?*	*rgf2:: KanMx6 pkd2::pkd2-B42-ura4+-his5+ leu1-32*	This study
QC-Y1085	*h?*	*eng1:: KanMx6 kanMX6-81xnmt1-pkd2*	This study
QC-Y1093	*h?*	*pkd2::pkd2-B42-ura4+-his5+ leu1-32 mok1-664*	This study
QC-Y1096	*h?*	*mok1-664 KanMX6-81xnmt1-pkd2*	This study
QC-Y1108	*h?*	*cwg1-2 pkd2::pkd2-B42-ura4+-his5+ leu1-32*	This study
QC-Y1109	*h?*	*cwg1-2 kanMX6-81xnmt1-pkd2*	This study
QC-Y1154	*h?*	*kanMX6-81xnmt1-pkd2 leu1-32 cdc7-GFP::ura4*	This study
QC-Y1162	*h+*	*agn1::kanMX6*	Bioneer
QC-Y1168	*h?*	*KanMX6-81xnmt1-pkd2 sid1-125 leu1-32 ade6-210*	This study
QC-Y1178	*h?*	*KanMX6-81xnmt1-pkd2 ace2::kanR*	This study
QC-Y1181	*h?*	*agn1::kanMX6 pkd2::pkd2-B42-ura4+-his5+ leu1-32*	This study
QC-Y1190	*h?*	*agn1::kanMX6 kanMX6-81xnmt1 pkd2*	This study
QC-Y1198	*h?*	*orb6-25 pkd2::pkd2-B42-ura4+-his5+ leu1-32*	This study
QC-Y1227	*h?*	*pkd2::pkd2-B42-ura4+-his5+ leu1-32 his5+:pact1:CRIB[gic2aa1-181]-3mCherry:bsdMX*	This study
QC-Y1250	*h+*	*mor2-282 (cps12-282) pkd2::pkd2-B42-ura4+-his5+ leu1-32*	This study
QC-Y1254	*h?*	*exo70Δ::kanMX6*	This study
QC-Y1256	*h?*	*pkd2::pkd2-B42-ura4+-his5+ leu1-32 exo70Δ::kanMX6*	This study
QC-Y1274	*h?*	*pkd2::pkd2-B42-ura4+-his5+ leu1-32 spg1-106*	This study
Qc-Y1307	*h?*	*cdc42-1625 pkd2::pkd2-B42-ura4+-his5+ leu1-32*	This study
QC-Y1352	*h?*	*sty1::kanMX6 pkd2::pkd2-B42-ura4+-hist5+ leu1-32*	This study
YDM4254	*h?*	*orb6-25 sid2-250*	Dannel McCollum
YDM4341	*h?*	*orb6-25 mob1-R4*	Dannel McCollum

References:

Balasubramanian, M.K., D. McCollum, L. Chang, K.C. Wong, N.I. Naqvi, X. He, S. Sazer, and K.L. Gould. 1998. Isolation and characterization of new fission yeast cytokinesis mutants. *Genetics*. 149:1265-1275.

Barr, M.M., and P.W. Sternberg. 1999. A polycystic kidney-disease gene homologue required for male mating behaviour in C. elegans. *Nature*. 401:386-389.

Beltraminelli, N., M. Murone, and V. Simanis. 1999. The S. pombe zfs1 gene is required to prevent septation if mitotic progression is inhibited. *J Cell Sci*. 112 Pt 18:3103-3114.

Bohnert, K.A., A.P. Grzegorzewska, A.H. Willet, C.W. Vander Kooi, D.R. Kovar, and K.L. Gould. 2013. SIN-dependent phosphoinhibition of formin multimerization controls fission yeast cytokinesis. *Genes Dev*. 27:2164-2177.

Bok, J.W., T. Sone, L.B. Silverman-Gavrila, R.R. Lew, F.J. Bowring, D.E. Catcheside, and A.J. Griffiths. 2001. Structure and function analysis of the calcium-related gene spray in Neurospora crassa. *Fungal genetics and biology : FG & B*. 32:145-158.

Cai, J., X. Song, W. Wang, T. Watnick, Y. Pei, F. Qian, and D. Pan. 2018. A RhoA-YAP-c-Myc signaling axis promotes the development of polycystic kidney disease. *Genes & development*. 32:781-793.

Camargo, F.D., S. Gokhale, J.B. Johnnidis, D. Fu, G.W. Bell, R. Jaenisch, and T.R. Brummelkamp. 2007. YAP1 increases organ size and expands undifferentiated progenitor cells. *Curr Biol*. 17:2054-2060.

Chen, Q., and T.D. Pollard. 2011. Actin filament severing by cofilin is more important for assembly than constriction of the cytokinetic contractile ring. *The Journal of cell biology*. 195:485-498.

Cortes, J.C., M. Sato, J. Munoz, M.B. Moreno, J.A. Clemente-Ramos, M. Ramos, H. Okada, M. Osumi, A. Duran, and J.C. Ribas. 2012. Fission yeast Ags1 confers the essential septum strength needed for safe gradual cell abscission. *The Journal of cell biology*. 198:637-656.

Das, M., D.J. Wiley, X. Chen, K. Shah, and F. Verde. 2009. The conserved NDR kinase Orb6 controls polarized cell growth by spatial regulation of the small GTPase Cdc42. *Curr Biol*. 19:1314-1319.

DeCaen, P.G., M. Delling, T.N. Vien, and D.E. Clapham. 2013. Direct recording and molecular identification of the calcium channel of primary cilia. *Nature*. 504:315-318.

Delling, M., P.G. DeCaen, J.F. Doerner, S. Febvay, and D.E. Clapham. 2013. Primary cilia are specialized calcium signalling organelles. *Nature*. 504:311-314.

Dey, S.K., and T.D. Pollard. 2018. Involvement of the septation initiation network in events during cytokinesis in fission yeast. *J Cell Sci*. 131.

Dong, J., G. Feldmann, J. Huang, S. Wu, N. Zhang, S.A. Comerford, M.F. Gayyed, R.A. Anders, A. Maitra, and D. Pan. 2007. Elucidation of a universal size-control mechanism in Drosophila and mammals. *Cell*. 130:1120-1133.

Fankhauser, C., J. Marks, A. Reymond, and V. Simanis. 1993. The S. pombe cdc16 gene is required both for maintenance of p34cdc2 kinase activity and regulation of septum formation: a link between mitosis and cytokinesis? *The EMBO journal*. 12:2697-2704.

Furge, K.A., K. Wong, J. Armstrong, M. Balasubramanian, and C.F. Albright. 1998. Byr4 and Cdc16 form a two-component GTPase-activating protein for the Spg1 GTPase that controls septation in fission yeast. *Curr Biol*. 8:947-954.

Garcia-Cortes, J.C., and D. McCollum. 2009. Proper timing of cytokinesis is regulated by Schizosaccharomyces pombe Etd1. *The Journal of cell biology*. 186:739-753.

Gibbs, E., J. Hsu, K. Barth, and J.W. Goss. 2021. Characterization of the nanomechanical properties of the fission yeast (Schizosaccharomyces pombe) cell surface by atomic force microscopy. *Yeast (Chichester, England)*.

Gonzalez-Perrett, S., K. Kim, C. Ibarra, A.E. Damiano, E. Zotta, M. Batelli, P.C. Harris, I.L. Reisin, M.A. Arnaout, and H.F. Cantiello. 2001. Polycystin-2, the protein mutated in autosomal dominant polycystic kidney disease (ADPKD), is a Ca2+-permeable nonselective cation channel. *Proceedings of the National Academy of Sciences of the United States of America*. 98:1182-1187.

Goss, J.W., S. Kim, H. Bledsoe, and T.D. Pollard. 2014. Characterization of the roles of Blt1p in fission yeast cytokinesis. *Molecular biology of the cell*. 25:1946-1957.

Goss, J.W., and C.B. Volle. 2020. Using Atomic Force Microscopy To Illuminate the Biophysical Properties of Microbes. *ACS Appl Bio Mater*. 3:143-155.

Goyal, A., and V. Simanis. 2012. Characterization of ypa1 and ypa2, the Schizosaccharomyces pombe orthologs of the peptidyl proyl isomerases that activate PP2A, reveals a role for Ypa2p in the regulation of cytokinesis. *Genetics*. 190:1235-1250.

Gupta, S., M. Govindaraghavan, and D. McCollum. 2014. Cross talk between NDR kinase pathways coordinates cytokinesis with cell separation in Schizosaccharomyces pombe. *Eukaryot Cell*. 13:1104-1112.

Gupta, S., S. Mana-Capelli, J.R. McLean, C.T. Chen, S. Ray, K.L. Gould, and D. McCollum. 2013. Identification of SIN pathway targets reveals mechanisms of crosstalk between NDR kinase pathways. *Curr Biol*. 23:333-338.

Hanaoka, K., F. Qian, A. Boletta, A.K. Bhunia, K. Piontek, L. Tsiokas, V.P. Sukhatme, W.B. Guggino, and G.G. Germino. 2000. Co-assembly of polycystin-1 and -2 produces unique cation-permeable currents. *Nature*. 408:990-994.

Hardy, E., and L. Tsiokas. 2020. Polycystins as components of large multiprotein complexes of polycystin interactors. *Cellular signalling*. 72:109640.

Hergovich, A. 2016. The Roles of NDR Protein Kinases in Hippo Signalling. *Genes (Basel)*. 7.

Hirata, D., N. Kishimoto, M. Suda, Y. Sogabe, S. Nakagawa, Y. Yoshida, K. Sakai, M. Mizunuma, T. Miyakawa, J. Ishiguro, and T. Toda. 2002. Fission yeast Mor2/Cps12, a protein similar to Drosophila Furry, is essential for cell morphogenesis and its mutation induces Wee1-dependent G(2) delay. *The EMBO journal*. 21:4863-4874.

Hou, M.C., D.J. Wiley, F. Verde, and D. McCollum. 2003. Mob2p interacts with the protein kinase Orb6p to promote coordination of cell polarity with cell cycle progression. *J Cell Sci*. 116:125-135.

Hsiang, T., and D.L. Baillie. 2005. Comparison of the yeast proteome to other fungal genomes to find core fungal genes. *J Mol Evol*. 60:475-483.

Huang, J., S. Wu, J. Barrera, K. Matthews, and D. Pan. 2005. The Hippo signaling pathway coordinately regulates cell proliferation and apoptosis by inactivating Yorkie, the Drosophila Homolog of YAP. *Cell*. 122:421-434.

Huang, K., D.R. Diener, A. Mitchell, G.J. Pazour, G.B. Witman, and J.L. Rosenbaum. 2007. Function and dynamics of PKD2 in Chlamydomonas reinhardtii flagella. *The Journal of cell biology*. 179:501-514.

Hughes, J., C.J. Ward, B. Peral, R. Aspinwall, K. Clark, J.L. San Millan, V. Gamble, and P.C. Harris. 1995. The polycystic kidney disease 1 (PKD1) gene encodes a novel protein with multiple cell recognition domains. *Nature genetics*. 10:151-160.

Jin, Q.W., and D. McCollum. 2003. Scw1p antagonizes the septation initiation network to regulate septum formation and cell separation in the fission yeast Schizosaccharomyces pombe. *Eukaryot Cell*. 2:510-520.

Jin, Q.W., S. Ray, S.H. Choi, and D. McCollum. 2007. The nucleolar Net1/Cfi1-related protein Dnt1 antagonizes the septation initiation network in fission yeast. *Molecular biology of the cell*. 18:2924-2934.

Jin, Q.W., M. Zhou, A. Bimbo, M.K. Balasubramanian, and D. McCollum. 2006. A role for the septation initiation network in septum assembly revealed by genetic analysis of sid2-250 suppressors. *Genetics*. 172:2101-2112.

Johnson, A.E., D. McCollum, and K.L. Gould. 2012. Polar opposites: Fine-tuning cytokinesis through SIN asymmetry. *Cytoskeleton (Hoboken)*. 69:686-699.

Karagiannis, J., R. Oulton, and P.G. Young. 2002. The Scw1 RNA-binding domain protein regulates septation and cell-wall structure in fission yeast. *Genetics*. 162:45-58.

Knapp, B.D., P. Odermatt, E.R. Rojas, W. Cheng, X. He, K.C. Huang, and F. Chang. 2019. Decoupling of Rates of Protein Synthesis from Cell Expansion Leads to Supergrowth. *Cell Syst*. 9:434-445 e436.

Lew, R.R. 2011. How does a hypha grow? The biophysics of pressurized growth in fungi. *Nat Rev Microbiol*. 9:509-518.

Li, Y., L. He, N.A.P. Gonzalez, J. Graham, C. Wolgemuth, D. Wirtz, and S.X. Sun. 2017. Going with the Flow: Water Flux and Cell Shape during Cytokinesis. *Biophysical journal*. 113:2487-2495.

Lima, W.C., A. Vinet, J. Pieters, and P. Cosson. 2014. Role of PKD2 in rheotaxis in Dictyostelium. *PLoS One*. 9:e88682.

Liu, P., X. Lou, J.L. Wingfield, J. Lin, D. Nicastro, and K. Lechtreck. 2020. Chlamydomonas PKD2 organizes mastigonemes, hair-like glycoprotein polymers on cilia. *The Journal of cell biology*. 219.

Liu, X., T. Vien, J. Duan, S.H. Sheu, P.G. DeCaen, and D.E. Clapham. 2018. Polycystin-2 is an essential ion channel subunit in the primary cilium of the renal collecting duct epithelium. *eLife*. 7.

Miettinen, T.P., J.H. Kang, L.F. Yang, and S.R. Manalis. 2019. Mammalian cell growth dynamics in mitosis. *eLife*. 8.

Minc, N., A. Boudaoud, and F. Chang. 2009. Mechanical forces of fission yeast growth. *Curr Biol*. 19:1096-1101.

Mochizuki, T., G. Wu, T. Hayashi, S.L. Xenophontos, B. Veldhuisen, J.J. Saris, D.M. Reynolds, Y. Cai, P.A. Gabow, A. Pierides, W.J. Kimberling, M.H. Breuning, C.C. Deltas, D.J. Peters, and S. Somlo. 1996. PKD2, a gene for polycystic kidney disease that encodes an integral membrane protein. *Science (New York, N.Y)*. 272:1339-1342.

Morris, Z., D. Sinha, A. Poddar, B. Morris, and Q. Chen. 2019. Fission yeast TRP channel Pkd2p localizes to the cleavage furrow and regulates cell separation during cytokinesis. *Molecular biology of the cell*. 30:1791-1804.

Moser, M.J., M.R. Flory, and T.N. Davis. 1997. Calmodulin localizes to the spindle pole body of Schizosaccharomyces pombe and performs an essential function in chromosome segregation. *Journal of cell science*. 110 (Pt 15):1805-1812.

Munoz, J., J.C. Cortes, M. Sipiczki, M. Ramos, J.A. Clemente-Ramos, M.B. Moreno, I.M. Martins, P. Perez, and J.C. Ribas. 2013. Extracellular cell wall beta(1,3)glucan is required to couple septation to actomyosin ring contraction. *The Journal of cell biology*. 203:265-282.

Palmer, C.P., E. Aydar, and M.B. Djamgoz. 2005. A microbial TRP-like polycystic-kidney-disease-related ion channel gene. *Biochem J*. 387:211-219.

Pan, D. 2007. Hippo signaling in organ size control. *Genes & development*. 21:886-897.

Pollard, T.D., and J.Q. Wu. 2010. Understanding cytokinesis: lessons from fission yeast. *Nature reviews*. 11:149-155.

Protchenko, O., R. Rodriguez-Suarez, R. Androphy, H. Bussey, and C.C. Philpott. 2006. A screen for genes of heme uptake identifies the FLC family required for import of FAD into the endoplasmic reticulum. *The Journal of biological chemistry*. 281:21445-21457.

Ray, S., K. Kume, S. Gupta, W. Ge, M. Balasubramanian, D. Hirata, and D. McCollum. 2010. The mitosis-to-interphase transition is coordinated by cross talk between the SIN and MOR pathways in Schizosaccharomyces pombe. *The Journal of cell biology*. 190:793-805.

Rigamonti, M., S. Groppi, F. Belotti, R. Ambrosini, G. Filippi, E. Martegani, and R. Tisi. 2015. Hypotonic stress-induced calcium signaling in Saccharomyces cerevisiae involves TRP-like transporters on the endoplasmic reticulum membrane. *Cell calcium*. 57:57-68.

Salimova, E., M. Sohrmann, N. Fournier, and V. Simanis. 2000. The S. pombe orthologue of the S. cerevisiae mob1 gene is essential and functions in signalling the onset of septum formation. *J Cell Sci*. 113 (Pt 10):1695-1704.

Schmidt, S., M. Sohrmann, K. Hofmann, A. Woollard, and V. Simanis. 1997. The Spg1p GTPase is an essential, dosage-dependent inducer of septum formation in Schizosaccharomyces pombe. *Genes Dev*. 11:1519-1534.

Silverman-Gavrila, L.B., and R.R. Lew. 2003. Calcium gradient dependence of Neurospora crassa hyphal growth. *Microbiology (Reading)*. 149:2475-2485.

Simanis, V. 2015. Pombe's thirteen - control of fission yeast cell division by the septation initiation network. *J Cell Sci*. 128:1465-1474.

Sohrmann, M., S. Schmidt, I. Hagan, and V. Simanis. 1998. Asymmetric segregation on spindle poles of the Schizosaccharomyces pombe septum-inducing protein kinase Cdc7p. *Genes & development*. 12:84-94.

Sparks, C.A., M. Morphew, and D. McCollum. 1999. Sid2p, a spindle pole body kinase that regulates the onset of cytokinesis. *The Journal of cell biology*. 146:777-790.

Stephenson, K.S., N.A. Gow, F.A. Davidson, and G.M. Gadd. 2014. Regulation of vectorial supply of vesicles to the hyphal tip determines thigmotropism in Neurospora crassa. *Fungal Biol*. 118:287-294.

Su, Q., F. Hu, X. Ge, J. Lei, S. Yu, T. Wang, Q. Zhou, C. Mei, and Y. Shi. 2018. Structure of the human PKD1-PKD2 complex. *Science*. 361.

Ta, C.M., T.N. Vien, L.C.T. Ng, and P.G. DeCaen. 2020. Structure and function of polycystin channels in primary cilia. *Cellular signalling*. 72:109626.

Tang, X., J. Huang, A. Padmanabhan, K. Bakka, Y. Bao, B.Y. Tan, W.Z. Cande, and M.K. Balasubramanian. 2011. Marker reconstitution mutagenesis: a simple and efficient reverse genetic approach. *Yeast*. 28:205-212.

Tatebe, H., K. Nakano, R. Maximo, and K. Shiozaki. 2008. Pom1 DYRK regulates localization of the Rga4 GAP to ensure bipolar activation of Cdc42 in fission yeast. *Curr Biol*. 18:322-330.

Tay, Y.D., M. Leda, C. Spanos, J. Rappsilber, A.B. Goryachev, and K.E. Sawin. 2019. Fission Yeast NDR/LATS Kinase Orb6 Regulates Exocytosis via Phosphorylation of the Exocyst Complex. *Cell reports*. 26:1654-1667 e1657.

Thevenaz, P., U.E. Ruttimann, and M. Unser. 1998. A pyramid approach to subpixel registration based on intensity. *IEEE Trans Image Process*. 7:27-41.

Verde, F., D.J. Wiley, and P. Nurse. 1998. Fission yeast orb6, a ser/thr protein kinase related to mammalian rho kinase and myotonic dystrophy kinase, is required for maintenance of cell polarity and coordinates cell morphogenesis with the cell cycle. *Proceedings of the National Academy of Sciences of the United States of America*. 95:7526-7531.

Volle, C.B., M.A. Ferguson, K.E. Aidala, E.M. Spain, and M.E. Nunez. 2008. Spring constants and adhesive properties of native bacterial biofilm cells measured by atomic force microscopy. *Colloids Surf B Biointerfaces*. 67:32-40.

Watnick, T.J., Y. Jin, E. Matunis, M.J. Kernan, and C. Montell. 2003. A flagellar polycystin-2 homolog required for male fertility in Drosophila. *Curr Biol*. 13:2179-2184.

Willet, A.H., A.K. DeWitt, J.R. Beckley, D.M. Clifford, and K.L. Gould. 2019. NDR Kinase Sid2 Drives Anillin-like Mid1 from the Membrane to Promote Cytokinesis and Medial Division Site Placement. *Curr Biol*. 29:1055-1063 e1052.

Wood, C.R., Z. Wang, D. Diener, J.M. Zones, J. Rosenbaum, and J.G. Umen. 2012. IFT proteins accumulate during cell division and localize to the cleavage furrow in Chlamydomonas. *PLoS One*. 7:e30729.

Wu, J.Q., J.R. Kuhn, D.R. Kovar, and T.D. Pollard. 2003. Spatial and temporal pathway for assembly and constriction of the contractile ring in fission yeast cytokinesis. *Developmental cell*. 5:723-734.

Wu, J.Q., V. Sirotkin, D.R. Kovar, M. Lord, C.C. Beltzner, J.R. Kuhn, and T.D. Pollard. 2006. Assembly of the cytokinetic contractile ring from a broad band of nodes in fission yeast. *The Journal of cell biology*. 174:391-402.

Yu, F.X., B. Zhao, and K.L. Guan. 2015. Hippo Pathway in Organ Size Control, Tissue Homeostasis, and Cancer. *Cell*. 163:811-828.